V²iFi: in-Vehicle Vital Sign Monitoring via Compact RF Sensing

TIANYUE ZHENG* and ZHE CHEN*, Nanyang Technological University, Singapore
CHAO CAI, Nanyang Technological University, Singapore
JUN LUO, Nanyang Technological University, Singapore
XU ZHANG, University of Chicago, United States

Given the significant amount of time people spend in vehicles, health issues under driving condition have become a major concern. Such issues may vary from fatigue, asthma, stroke, to even heart attack, yet they can be adequately indicated by vital signs and abnormal activities. Therefore, in-vehicle vital sign monitoring can help us predict and hence prevent these issues. Whereas existing sensor-based (including camera) methods could be used to detect these indicators, privacy concern and system complexity both call for a convenient yet effective and robust alternative. This paper aims to develop V²iFi, an intelligent system performing monitoring tasks using a COTS impulse radio mounted on the windshield. V²iFi is capable of reliably detecting driver's vital signs under driving condition and with the presence of passengers, thus allowing for potentially inferring corresponding health issues. Compared with prior work based on Wi-Fi CSI, V²iFi is able to distinguish reflected signals from multiple users, and hence provide finer-grained measurements under more realistic settings. We evaluate V²iFi both in lab environments and during real-life road tests; the results demonstrate that respiratory rate, heart rate, and heart rate variability can all be estimated accurately. Based on these estimation results, we further discuss how machine learning models can be applied on top of V²iFi so as to improve both physiological and psychological wellbeing in driving environments.

CCS Concepts: • **Applied computing** → **Consumer health**; • **Hardware** → *Sensor applications and deployments*; • **Human-centered computing** → Ubiquitous and mobile computing systems and tools.

Additional Key Words and Phrases: In-Vehicle Health Monitoring, Vital Signs, Impulse Radio, Ultra Wideband

1 INTRODUCTION

With the rapid development of artificial intelligence, vehicles are becoming increasingly "smart" nowadays: they not only learn to drive by itself, but also attempt to better understand and interact with the driver and passengers. In particular, health monitoring is one of the essential components of intelligent vehicles; it aims to figure out the health status of people under driving condition, especially after long hours of daily commutes and frustrating traffic jams [21]. For example, drowsy driving has been reported to have caused 25% fatal vehicle

---

*Both authors contributed equally to this research.

Authors' addresses: Tianyue Zheng, tianyue002@e.ntu.edu.sg; Zhe Chen, chen.zhe@ntu.edu.sg, Nanyang Technological University, Singapore; Chao Cai, chris.cai@ntu.edu.sg, Nanyang Technological University, Singapore; Jun Luo, junluo@ntu.edu.sg, Nanyang Technological University, Singapore; Xu Zhang, zhangxu@uchicago.edu, University of Chicago, Chicago, United States.

crashes [26], and vital signs such as respiration and heartbeat are important indicators for early detection of drowsiness [13, 52]. Consequently, an in-vehicle health monitoring system that keeps watching these indicators offers both the vehicle and driver better perception and decision-making capabilities, thus leading to a healthy and safe driving experiences.

To enable healthy and safe driving, automotive companies have built various monitoring system, including ATTENTION ASSIST® by Mercedes-Benz [17], Driver Alert Control (DAC) by Volvo [57] and SmartSenior by BMW [7]. In the meantime, research groups from around the world have also been attracted to this topic [3, 9, 12, 30, 35, 62]. By far, two main categories of such systems work on monitoring person (driver in particular) directly, namely camera-based [12, 30, 57] and wearable sensor-based [3, 9, 35] (e.g., EEG and ECG). Although these approaches work well technically, they may not be exactly practical in real life, because of well-known weaknesses including privacy concern, poor performance in low-light, as well as the use of intrusive sensors (causing uncomfortable user experience).

Fortunately, recent progress in wireless sensing has brought us new hope to overcome the aforementioned weaknesses [2, 36, 59, 63]. Such a system always transmits wireless (e.g., radio and acoustic) signals and captures their reflections. As the reflections off persons carry their respective vital signs,[1] one may extract these vital signs from the reflections without intrusive sensors touching human bodies, while respecting the privacy of users and avoiding the interference of ambient light. However, different from the state-of-the-art wireless based vital sign monitoring, in-vehicle monitoring is much more complicated because of the confined and noisy nature of driving environments. To tackle these challenges, there have been a few existing studies on in-vehicle monitoring of either general health or specific vital signs via acoustic [62] or Radio Frequency (RF) [32] signals. Although acoustic signals can deliver vital sign monitoring ubiquitously via smart devices such as smartphones [62], they are prone to be contaminated by background sounds under driving condition. Moreover, babies and pets may feel uncomfortable as they are sensitive to the high frequency acoustic signals used by acoustic sensing.

Compared with acoustic signals, RF signals are even less sensitive to ambient noises such as heat and sounds, hence it poses a more promising solution for in-vehicle monitoring. WiFind [32] leverages Channel State Information (CSI) of Wi-Fi devices to detect driver motions and respiratory rate, based on which fatigue state could potentially be inferred. However, it only offers coarse-grained measurements due to its narrow Wi-Fi bandwidth. To make things worse, the system may fail in the presence of multiple persons in the vehicle. In order to better illustrate this latter issue, we use Wi-Fi card Intel 5300 [29] to detect respiratory waveform in a vehicle. Whereas the respiratory waveform of a driver alone can be clearly identified in Fig. 1(a), the periodic feature of this waveform is corrupted and cannot be easily distinguished when multiple passengers are present, as shown in Fig. 1(b). The reason is that the narrow Wi-Fi bandwidth cannot support high temporal resolution in such an extreme multipath environment. Note that differentiating multiple persons via their respective respiratory rates does not help, as identifying the critical monitoring target (e.g., the driver) is still impossible without position information, and the respiratory rates can be similar even for different persons. As a teaser to our work, Fig. 1(c) demonstrates that, when properly used, an impulse radio with ultra-wideband offers a much higher temporal resolution, and hence can readily differentiate multiple persons based on their relative distances, and then focus on monitoring the driver. Last but not least, using standard Wi-Fi radio for sensing purpose may affect its normal data communication function, and the resulted setting is *bistatic* (i.e., transmitter and receiver are separated [46]); these all make it difficult to test and deploy a system.

To summarize, in order to further improve the performance of driver vital sign monitoring system based on RF sensing, we face the following challenges that largely confine the capability of existing systems:

---

[1]As vital signs are actually micro-scale body activities, the ability to monitor the former implies the same to the latter. Therefore, our technical discussions focus only on vital sign monitoring for the sake of conciseness.

- **Deployment complexity.** In-vehicle vital sign monitoring based on Wi-Fi CSI requires an Access Point (AP) and a STAtion (STA) [32]. Such a bistatic system is too complicated to be adopted as an intelligent component of smart vehicles in practice.
- **Passenger interference.** Previous research works based on Wi-Fi CSI are not robust to the cases where multiple persons are in a vehicle. Respiratory movements caused by other passengers in the cabin can distort the CSI and worsen the performance.
- **Excessive noise.** Previous vital sign monitoring systems are mostly designed for a home setting [2, 63]. Performance of in-vehicle vital sign monitoring can deteriorate with the presence of excessive noise caused by the running vehicle and moving human body parts.
- **Low sensitivity.** Technologies based on Wi-Fi CSI cannot ensure sufficient temporal resolution because of the narrow bandwidth. Therefore, measurements of vital signs using Wi-Fi CSI cannot be very accurate, especially given the vibration background created by engines and road conditions.

To answer these challenges, we propose V²iFi as a compact in-**Ve**hicle **Vi**tal sign monitoring system endowed with fine-grained sensitivity. It consists of low-cost Commercial Off-The-Shelf (COTS) components, and is hence readily deployable, as illustrated in Fig. 2. V²iFi can filter the interference from passengers and vibrations caused by moving vehicles while focusing on driver's vital sign monitoring. The reconstructed RF signals induced by vital signs can then be used to estimate respiratory rate, heart rate, and even finer-grained heart rate variability. As V²iFi offers continuous monitoring on driver's vital signs, we will be able to perform real-time and comprehensive

(a) Wi-Fi monitoring for driver alone. (b) Wi-Fi monitoring with multiple persons. (c) Impulse radio with multiple persons.
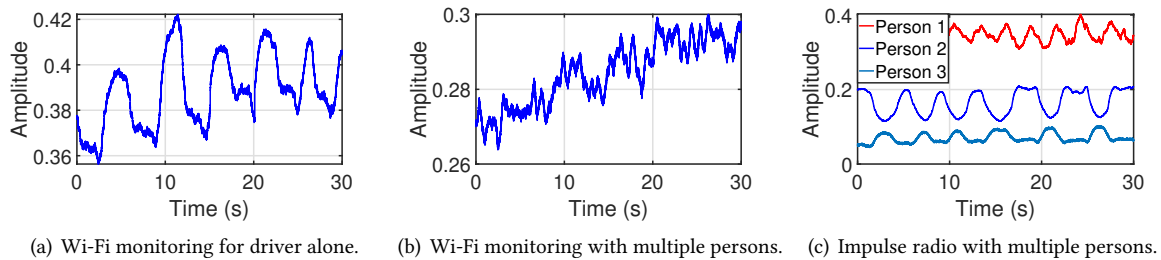
Fig. 1. Drivers' respiratory waveform can be detected without any other person using Wi-Fi CSI shown in (a). However, (b) illustrates that multiple persons degrade the respiratory waveform of driver due to narrow band Wi-Fi in the rich multipath in-vehicle environment. Instead, V²iFi leverages a COTS impulse radio to distinguish multiple persons, so as to further filter out multiple persons' interference as demonstrated in (c).

Fig. 2. A vital signs monitoring scenario of driving vehicle. The driver's RF reflections always contains his or her vital signs with noise introduced by vehicle's vibrations. V²iFi separates such vibrations to reconstruct signals of vital signs.

diagnosis of the health status of the driver. Particularly, we should be able to detect driver drowsiness in its early stage and hence prevent vehicle accidents.
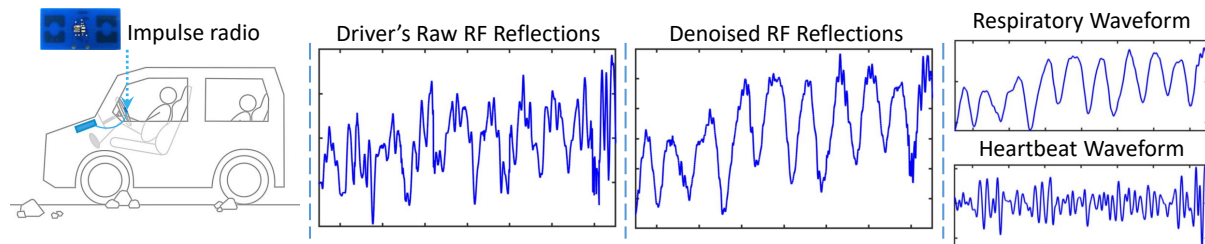
Specifically, V²iFi employs a COTS impulse radio to collect RF reflections from people. The COTS impulse radio is compact and *monostatic* (i.e., the transmitter and receiver are co-located [46]); it can be readily integrated with embedded devices such as Raspberry Pi [47] adopted by us to form an edge computing node, rendering a straightforward in-vehicle deployment shown in Fig. 2 (leftmost). The radio's ultra-wideband enables us to develop algorithms that accurately sorts out signals reflected from different people under complex multipath conditions. This further allows us to zoom in and inspect the RF reflections from the driver and hence extract his/her vital signs. In addition, the competent sensitivity of V²iFi delivers abundant information for combating other background noises. Leveraging this capability, our new Multi-Sequence Variational Mode Decomposition (MS-VMD) algorithm decomposes a set of related time series into multiple band-separated intrinsic modes. This enables V²iFi to filter out noises such as vibrations of vehicle, reconstruct both respiratory and heartbeat waveforms, and in turn estimate respiratory rate, heart rate, and even heart rate variability accordingly. In summary, our major contributions in this paper are:

- Our hardware design for V²iFi innovatively combines a COTS impulse radio with a compact edge computing platform. Leveraging the high temporal resolution offered by an impulse radio, V²iFi is able to distinguish signals reflected from various users and hence focus on monitoring the driver. Moreover, compared with existing wireless solutions (e.g., [32]), V²iFi is convenient to deploy thanks to its low system complexity, making it a practical system for complicated driving environments.
- We emphasize on the robustness in vital sign monitoring to overcome noise in driving environments. To prepare the signal for vital sign extraction, V²iFi uses a combination of filters to remove noise and improve signal quality, it then detects and discards unstable data frames corrupted by noise. As a result, V²iFi can extract vital sign information from noisy data frames to the largest extent.
- We develop a novel MS-VMD algorithm to fully leverage the wide bandwidth of the UWB signal and perform signal separation via optimization techniques. The MS-VMD algorithm allows V²iFi to jointly extract vital signs from multiple sequences of signals. This enables V²iFi to accurately estimate driver's vital signs carried by reflected signals, including even the subtle heart rate variability, which, to the best of our knowledge, has never been extracted by wireless sensing under driving condition.
- We conduct extensive experiments to evaluate the performance of V²iFi under various conditions. All the results demonstrate that V²iFi is robust to various unfavorable factors including bumpy road and heavy clothing of the driver, proving its outstanding effectiveness in practice.

The rest of the paper is organized as follows. Sec. 2 explains the vital signs to be measured by V²iFi. Sec. 3 presents the system design of V²iFi. Sec. 4 reports the evaluation results. Limitations and potentials are discussed in Sec. 5. Sec. 6 gives a brief review of related work. Sec. 7 concludes this paper.

2 VITAL SIGNS AS HEALTH INDICATORS IN DRIVING ENVIRONMENTS

Before proceeding to present our system details, we first discuss the measurable vital signs as health indicators in driving environments. The essential idea is to provide a necessary background and strong motivation for the development of V²iFi, in the sense of which vital signs can be quantitatively measured and how they are relevant to personal health status. Basically, we propose adopting the following dimensions: i) respiratory rate: the number of breaths a person takes per minute, ii) heart rate: the number of times a person's heart contracts and relaxes per minute, and iii) heart rate variability (HRV): the physiological phenomenon of variation in time intervals between heartbeats. All these can be measured by V²iFi's impulse radio, and they are closely related to personal health status.

2.1 Respiratory Rate and Heart Rate

Respiratory rate is one of the crucial indicators of a person's health issues. Abnormal respiratory rate under 12 breaths-per-minute (bpm) or over 25 bpm has been shown to be an important predictor of health issues, such as asthma [10], anxiety [28], pneumonia [53], lung disease [14], heart disease [15, 25] and drug overdose. In particular, Solaz et al. [52] observe abnormal change in respiratory rates and use it to infer abnormal health issues like driver drowsiness. Lisper et al. [37] report that, during a long-time continuous driving, respiratory rate of the driver and passengers are found to have slowed down gradually. Similarly, irregular heart rate is also a crucial indicator of serious health issues such as cardiac disease [16, 40]. Also, Sharma et al. [51] show that irregular heart rate is a sign of electrolyte imbalance. In terms of driving environments, Jo et al. [33] demonstrate that heart rate significantly decreases during sleepy driving. Banning et al. [4] report that people with irregular heartbeat are more likely to cause a traffic accident.

The aforementioned discussions have clearly shown the relevance of both respiratory rate and heart rate as indicators for driving-specific health status (e.g., driver fatigue, drunk driving), so they should be chosen as key vital signs for in-vehicle monitoring, yet we would need to avoid using intrusive sensors that cause uncomfortable user experience. Recently progress in RF sensing provide us with an alternative solution for remotely extracting these vital signs. Zeng et al. [63] design a Wi-Fi based system for respiration detection, and Adib et al. [2] demonstrate that respiratory rate and heart rate can both be measured remotely by leveraging an FMCW radio. In particular, for the driving environments, Peng et al. [32] has migrated the Wi-Fi based for estimating respiratory rate, while Park et al. [44] design a special RF sensor for monitoring both respiratory rate and heart rate of the driver. However, it is still not clear if these proposals may effectively handle realistic scenarios with multiple passenger present.

2.2 Heart Rate Variability

It is well known that a healthy heart does not beat at a regular interval [50]. In other words, the rhythms of a healthy heart are not as stable as heart rate; they are instead non-linear and offer a higher-dimensional information. Therefore, it is a more useful indicator of a personal health status than respiratory and heart rates. Variations in heart beat intervals are controlled by the unconscious part of human nervous system, i.e., the Automatic Nervous System (ANS) [24]. This part of the nervous system regulates heart beat, respiration, pupillary response, urination, sexual arousal and digestive process. The ANS can be further divided into two sub-systems, i.e., sympathetic and parasympathetic nervous system. Human heart without external input will beat at constant rate of approximately 100 bpm. However, the two nervous subsystems compete with each other, influencing nerves in heart tissues and causing variations in heart beat intervals. Therefore, HRV clearly reflects the general state of the nervous system and thus personal health status.

Specifically, HRV has been used to detect multiple health issues. In [48], Sessa et al. report abnormal HRV precedes sudden cardiac attack. In [27], Fujiwara et al. demonstrate that changes in sleep patterns affect nervous system, and HRV changes as a result. In another study, Benichou et al. [5] show that type 2 diabetes cause significant decrease in HRV. HRV is also shown to be linked to asthma [38], anxiety [11] and drug overdose [60]. Similar to respiratory rate and heart rate, HRV can also be obtained from reflected RF signals. Although HRV signal is weak and hard to capture, Zhao et al. [65] demonstrated that ECG-like HRV signal can be extracted from mixed signal of heartbeat and respiration using numerical differentiation. Whereas their findings have confirmed the existence of HRV signal in the reflected RF signal, their method may not be robust to noise and interference under driving conditions, so we require a novel estimation algorithm for V²iFi.

In brief, HRV is particularly useful for indicating health status in any environments, and it can be obtained from RF signals, so we choose it to be one of the key vital signs for V²iFi. However, there are multiple indices that describe HRV, and they can be categorized into categories summarized in Table 1 [49]. Some of these indices

Table 1. A summary of HRV measurements.

Category	Parameters
Time Domain	Interbeat Interval (IBI), SDNN, SDRR, SDANN, SDNN index (SDNNI), pNN50, HR Max - HR Min, RMSSD, HRV triangular index
Frequency Domain	ULF power, VLF power, LF peak, LF power, HF peak, HF power, LF/HF
Non-linear	SD1, SD2, SD1/SD2, ApEn, SampEN, DFAα1, DFAα2, D_2

require complex computation and processing (e.g., ECG-like waveform). In our work, as RF signal only carries temporal information about heartbeats. We choose Interbeat Interval (IBI) as the HRV index. In fact, some other indicators, such as SDNN, SDRR and LF/HF, can be derived from IBI.

3 SYSTEM DESIGN OF V²IFI

V²iFi is composed of two hardware components, a single-board computer and an impulse radio, as well as backend algorithms for signal processing. It utilizes RF signals transmitted by the impulse radio for vital sign monitoring. Upon receiving the reflected signals, delicate procedures are taken to distill the targeted vital signs out of them, notably by our novel MS-VMD algorithm. In the following, we first provide a software system overview in Sec. 3.1, while leaving the explanations for hardware components to Sec. 4.1. Then we present the RF channel model in Sec. 3.2 and discuss algorithms for signal prepossessing, signal separation, and vital sign extraction in Sec. 3.3, 3.4, and 3.5, respectively.
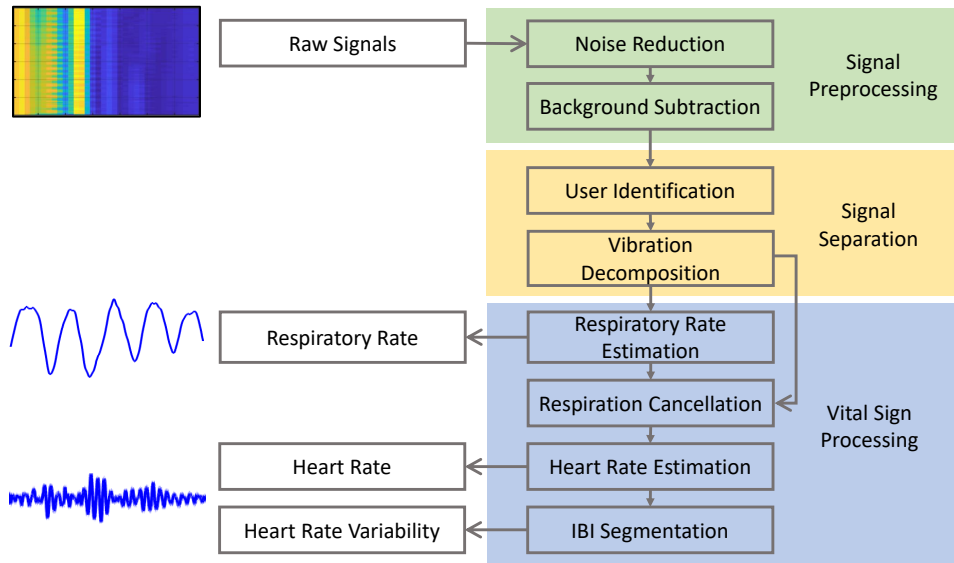
Fig. 3. Software system design of V²iFi.

3.1 Software System Overview

V²iFi's software architecture is illustrated in Fig. 3. The whole system consists of three components: signal preprocessing, signal separation, and vital sign processing.

- *RF signal preprocessing component.* This component includes noise reduction and background subtraction. After the reflected signal is received by the radio, the data is forwarded to the embedded computer for processing. Due to low power of the wideband Guassian pulse (−41 dBm/MHz) [42], we need to improve the SNR of signals. Basically, we employ smooth filter to reduce noise in the signals. Then, we utilize a loopback filter to remove the static reflections from clutters for background subtraction.
- *Signal separation component.* The greatest difficulty of in-vehicle vital sign estimation is how to remove the noise caused by vibrations of vehicle from the reflectors. We perform two steps to eliminate the vibration. First, we locate the driver, and extract driver-specific signals. Second, we propose a novel MS-VMD algorithm to decompose the mixed signals containing vibration noises and vital signs via leveraging the reflections from multiple body parts (i.e., signals from different fast-time bins).
- *Vital sign processing component.* After decomposing the signals, V²iFi identifies respiration and heartbeat signals from them. Next, V²iFi can estimate vital signs like respiratory rate, heart rate, and IBI. Together with all of them can be used to determine health issues of the driver.

We will model RF channel first, and elaborate on all components of V²iFi in the next few sections.

3.2 Modeling RF Channel

In this section, we introduce the theory of RF modeling of the impulse radio. V²iFi utilizes a system-on-chip impulse radio for transmitting and receiving wireless pulses. The system diagram of V²iFi is illustrated in Fig. 4. The transmitted signal is $s_k(t)$, the modulated signal is $x_k(t)$, the signal after passing the channel is $y_k(t)$, and the demodulated signal is $y_k^b(t)$. The architecture of the impulse radio is slightly different from traditional architecture [41]: it only employs an in-phase single-carrier frequency $\cos(2\pi f_c t)$ for upconversion, but In-phase and Quadrature (IQ) sampling ($\cos(2\pi f_c t)$ and $\sin(2\pi f_c t)$) at the receiver side for downconversion.
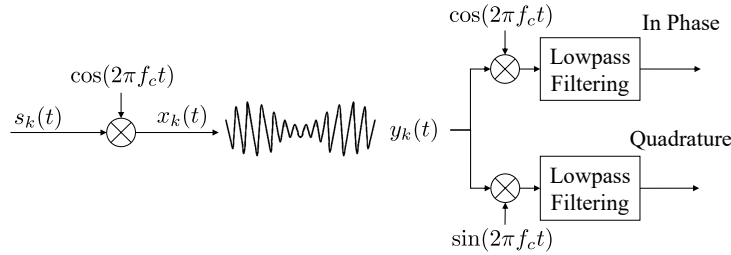

Fig. 4. System diagram from the baseband transmitted signal $s_k(t)$ to the baseband received signal $y_k^b(t)$.

The Gaussian pulse transmitted by V²iFi can be expressed by the following equation: $s(t) = V_{tx} \exp\left(-\frac{(t - \frac{T_p}{2})^2}{2\sigma_p^2}\right)$ where the amplitude of the pulse is V_{tx}, T_p is the duration of the signal, and σ_p^2 is the variance corresponding to the -10 dB bandwidth, actually we have $\sigma_p = \frac{1}{2\pi B_{-10dB}(\log_{10}(e))^{1/2}}$. After upconversion, the transmitted signal in time domain is given by:

$$x_k(t) = s(t - kT_s) \cdot \cos(2\pi f_c(t - kT_s)), \tag{1}$$

where f_c is carrier frequency, $T_s = \frac{1}{f_p}$ is duration of frame where f_p is the pulse repetition frequency, k denotes the k-th frame. Because the impulse radio transmits a sequence of identical pulses, we have $s(t - kT_s) = s(t)$. For simplicity, we can denote $t = t' + kT_s$ with $t' \in [0, T_s]$, and E.q. (1) can be written as $x_k(t) = s(t) \cdot \cos(2\pi f_c t)$.
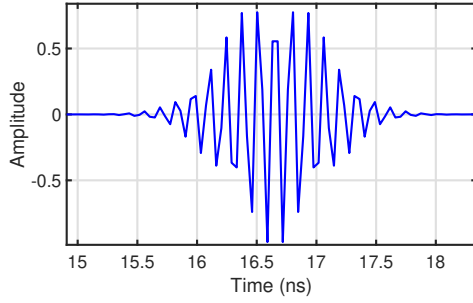
Fig. 5. Transmitted $x_k(t)$ in time domain.
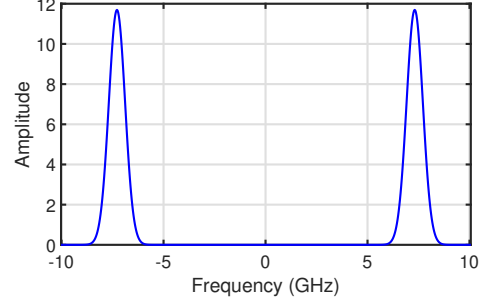
Fig. 6. Transmitted $x_k(t)$ in frequency domain.

The transmitted signal $x_k(t)$ is illustrated in Fig. 5, and its representation in the frequency domain is shown in Fig. 6. It can be seen that the carrier frequency is 7.3 GHz, and bandwidth is 1.4 GHz.

The impulse response $h_k(t)$ of the in-vehicle environment is given by: $h_k(t) = \sum_{p=1}^{P} \alpha_p \delta \left(t - \tau_p - \tau_p^D(kT_s) \right)$ where α_p is the channel gain of the pth reflection path signal in the vehicle, τ_p is the time delay of the p-th path, $\tau_p^D(kT_s)$ is the time delay caused by Doppler frequency shift of the p-th path. Moreover, for the impulse radio used in V²iFi , $\tau_p = \frac{2R_p}{c}$ and $\tau_p^D(kT_s) = \frac{2v_p kT_s}{c}$, where R_p is the distance between the target to be detected and the UWB radio, c is the speed of light, v_p is the speed of the moving target. The range resolution of V²iFi is given by $\Delta r = \frac{c}{2B}$ where B is the bandwidth of the impulse radio. Therefore, the time resolution of V²iFi can be calculated as $\Delta \tau = \frac{1}{2B}$.

In summary, the received signal of the impulse radio is:

$$y_k(t) = h_k(t) * x_k(t) = \sum_{p=1}^{P} \alpha_p \cos(2\pi f_c(t - kT_s - \tau_p - \tau_p^D(kT_s)) \cdot s(t - kT_s - \tau_p - \tau_p^D(kT_s)) + n(t), \qquad (2)$$

where $n(t)$ is Gaussian noise with a variance of ϵ^2, and the symbol $*$ denotes convolutional operation.

In a radar system, Pulse Repetition Interval (PRI) is the time between two consecutive pulses. We place the reflected signal of the same pulse in the same row, for example, the reflected signal of the first pulse in the first row, the reflected signal of the second pulse in the second row. We define the dimension of the row as the "fast-time" dimension, that is, the dimension of time slots composing a single PRI, and define the dimension of the column as the "slow-time" dimension, which updates every PRI [6].

By transforming the time sequence of the signal into a matrix, the idea of "fast-time" and "slow-time" can be visualized, as shown in Fig. 7, and an example of real received signals from UWB radio are illustrated in Fig. 8. Generally speaking, the fast-time dimension denotes time delays of range distance, and the slow-time axis is used to estimate Doppler effect by observing over a long time span. Hereafter, we abuse the terminology by using *sequence* to denote the vector of a ranging distance in the fast-time, such as a column vector in Fig. 7.

Received baseband signals $y_k^b(t)$ are obtained after applying IQ downconversion, we have:

$$y_k^b(t) = \sum_{p=1}^{P} \alpha_p e^{2\pi f_c(\tau_p + \tau_p^D(kT_s))} \cdot s(t - kT_s - \tau_p - \tau_p^D(kT_s)) + n(t). \qquad (3)$$

Let $t = lT_n$ represent l-th discrete samples obtained from ADC where T_n is the sampling interval. Then the discrete baseband signals can be represented by $y_k^b(lT_n)$. E.q. (3) indicated that different minute movements
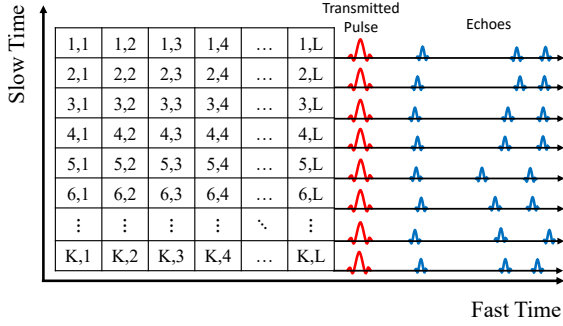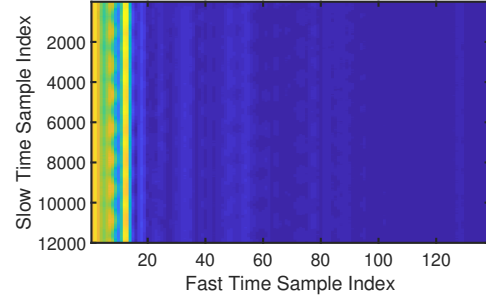
Fig. 7. The matrix of received baseband signals.

Fig. 8. An example of received baseband signals.

caused by vital signs in the vehicle have different τ_p and $\tau_p^D(kT_s)$ in $y_k^b(t)$. By utilizing the differences, different vital signs can be distinguished.

3.3 RF Signal Preprocessing

Before extracting information from RF signals, the effects from hardware or environment should be removed to guarantee signal quality. The RF signals preprocessing has two main steps: i) noise reduction and ii) background subtraction.

3.3.1 Noise Reduction. The received baseband signals are polluted with noise, as shown in Fig. 9. Noise will prevent the following vital signs extraction modules to work properly. Especially, vital signs will be immersed in noise. Therefore, a cascading filter comprised of a low-pass Finite Impulse Response (FIR) filter and a smoothing filter are utilized to enhance the SNR of the signals. The order of the designed FIR filter is 26 and Hamming window is used. The smooth filter with a window size of 50 points is used to further smooth the output signal of the FIR filter. Fig. 10. illustrates the output of the cascading filter. It can be seen that noise is suppressed.

Fig. 9. Received signal without SNR enhancement.
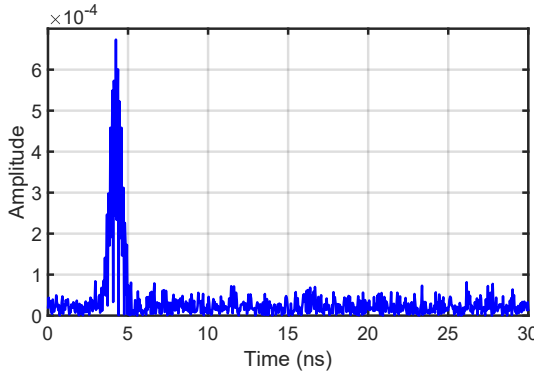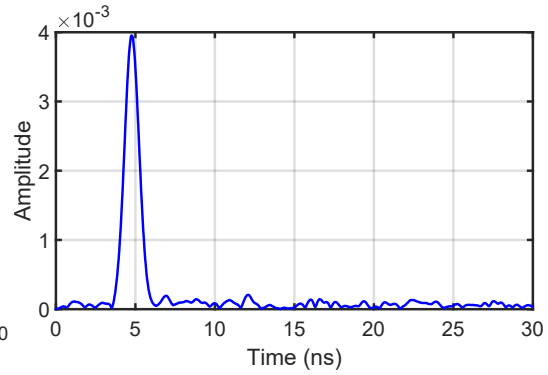

Fig. 10. Received signal with SNR enhancement.

3.3.2 Background Subtraction. Background subtraction removes all static reflectors in the background. Reflectors includes static and moving objects. Therefore, besides reflected signal from the human body, there are many sources of unwanted static signals reflected in the vehicle shown in Fig. 11. Unwanted signals in a radar are

generally described as noise and clutter. Loopback filters can be used to remove clutter from the original signal [1]. The clutter of the system can be described as: $c_k(t) = \beta c_{k-1}(t) + (1 - \beta)r_k(t)$ and the background subtracted signal can be represented as $y_k(t) = r_k(t) - c_k(t)$. In which β is a constant used for weighting, $r_k(t)$ is the value at k-th frame. We can see that the signal after background subtraction is illustrated in Fig. 12, where the clutters have been removed. A low β value enables the filter to remove background fast, but the filter is not robust to noise. On the other hand, a high β value makes background removal slow, but the process is robust to noise. In our work, β is set to 0.97.
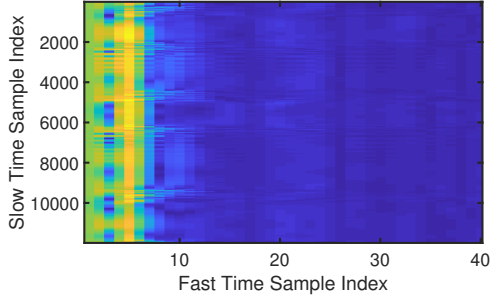

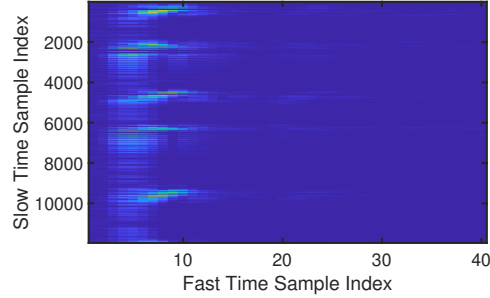Fig. 11. Signal before background subtraction.

Fig. 12. Signal after background subtraction.

3.4 Signal Separation

3.4.1 User Identification.
User identification is the process of identifying the driver's vital sign signal hidden in the radar data frames. It enables us to focus on the driver's signal for further vital sign extraction. The diagram of the user identification process is shown in Fig. 13.

The first step of user identification is to filter out the radar data frames that are unsuitable for user identification and further processing. In the diagram, we can see that fast movements in the driving environments degrade vital sign signals greatly. To combat this, we take out 5s data and 20s matrix from the input radar data frames, and these two matrices are called the short observation o_s and long observation o_l. We perform FFT along the slow-time axes of the two matrices to get the Doppler map of the long observation and short observation respectively. The Doppler map of the long observation is used for vital sign extraction, and the Doppler map of the short observation is used to detect fast movement.

By our definition, $b = \frac{\alpha_{\text{peak}}}{\sum_i \sum_j \alpha_{ij}/(I \times J)}$ is the measure of relative signal strength, where i denotes the i-th fast-time index, j denotes the j-th frequency index, α_{peak} is the peak amplitude on the Doppler map, and α_{ij} is the amplitude at fast-time index i and frequency index j, I is the total number of fast-time indices, and J is the total number of frequency indices, hence b_s (i.e., b of the short observation) is a measure of the relative strength of fast movement signal, and b_l (i.e., b of the long observation) is a measure of the relative strength of vital sign signal. $b_s > c \times b_l$, where c is empirically set to 1.2, is an empirical formula based on our experiments, it indicates that fast movement signal dominates vital sign signal. When this happens, the received signal is not stable and no valid vital signs can be extracted, hence we remove invalid frames. Otherwise, if there is no fast movement, peak detection algorithm is further used to locate the driver on the Doppler map.

The peak detection algorithm uses an adaptive threshold to detect real peaks where humans exist, it determines the best threshold above which any peak can be considered to be from the desired target. A sliding window is used to scan all values and estimate the noise threshold near the fast-time sample indices under test. The window size is set to $60\,\text{cm} \times 0.16\,\text{Hz}$, where 60 cm is the width of the human body and 0.16 Hz is the maximum difference
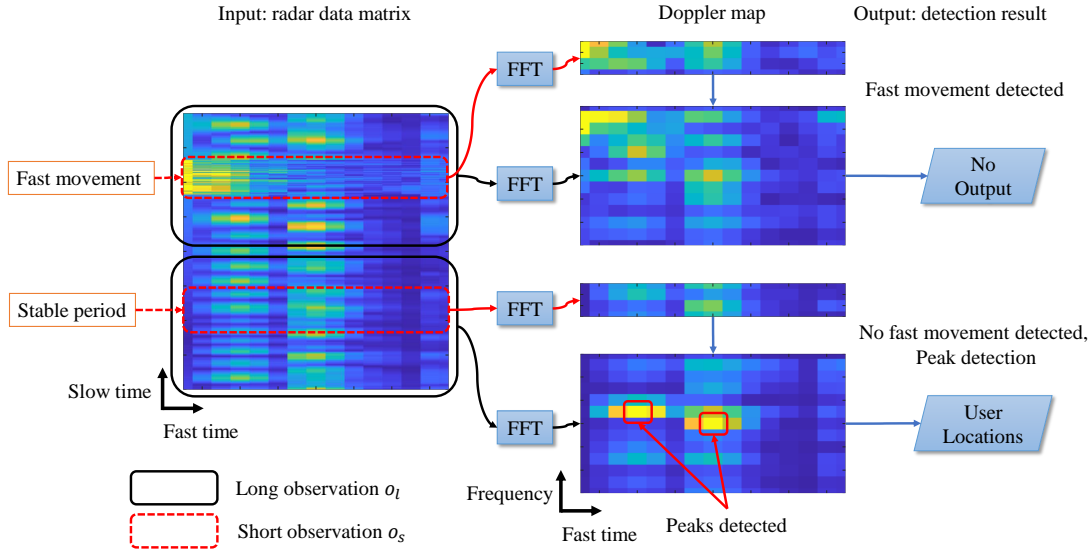
Fig. 13. The diagram of the user identification process. In the diagram, FFT means column-wise FFT, i.e., FFT along the slow-time axis.

of a specific person's respiratory rate. For example, if two peak indices are separated by a distance less than 60 cm, we only pick the peak index with higher amplitude. Last, we output the range value of the detected peak, which defines the location of the driver.

That algorithm is illustrated in Fig. 14. It can be seen that the noise floor threshold th_{motion} can be estimated by averaging the values around the fast-time index under test, and the value val of the fast-time bin under test is compared with $coef \cdot th_{\text{motion}}$ where $coef$ is a constant coefficient. Empirically, $coef$ is set to 1.5 in V²iFi . In Fig. 13, we can see that the peaks circled in red represent users occupying a fast-time index (range) and a frequency, hence the peaks can be used to identify different users.
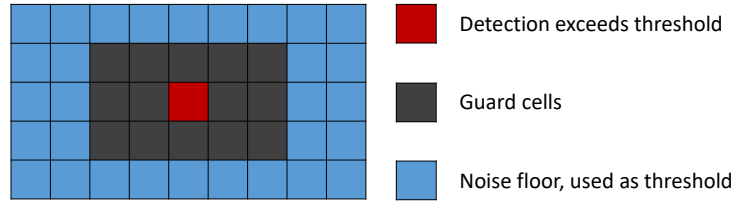
Fig. 14. The procedure of peak-average detection algorithm.

3.4.2 Vibration Decomposition via Variational Mode Decomposition. V²iFi separates breathing and heartbeat signals from noise in driving environments by utilizing the novel MS-VMD algorithm proposed by us, and further estimates respiratory rate, heart rate and fine-grained IBIs. Although we separate each people and identify the driver, vibrations of the vehicle always influences the vital sign estimation. The received signal contain mainly four components [62].

- *Respiration of the driver.* The respiration frequency of an adult ranges from 0.16 Hz to 0.6 Hz.

- *Heartbeat of the driver.* The heartbeat frequency of an adult ranges from 1 Hz to 2 Hz.
- *The vehicle's vibrations.* Frequency of vibrations of a running vehicle, caused by engine, transmission, wheel and bumps on the road ranges from 0.5 Hz to 10 Hz.
- *Vibrations of driver's motions.* Frequency of human motions such as turning steering wheel may bring interference with ranges from 0.5 Hz to 2 Hz.

We can see that the four components of the received signal are overlapping in frequency, hence a simple band-pass filter with specified frequency range cannot filter out undesired noise caused by vibrations. Although the vibrations of driver's motions may be separated via distances, there are some cases where the motions and vital signs occur at the same distance.

To separate the vital sign signals from other interference, VMD algorithm is used to decompose the signal into various modes by calculus of variation. Each mode of the signal is assumed to be around a central frequency and have a narrow bandwidth. VMD calculates these central frequencies and the mode functions concurrently, by using an optimization technique called Alternating Direction Method Method of Multipliers (ADMM). However, the VMD only supports single "sequence" decomposition (terminology defined in Sec. 3.2). Due to the complicated in-vehicle environment, a single sequence of signal may not be enough to extract vital signs, so we need to combine multiple sequences to enable accurate vital sign extractions. Therefore, to better refine the vital signs of the driver, we hereby design a Multi-Sequence VMD (MS-VMD) algorithm, an enhanced version of the conventional VMD algorithm.

It is noticed that in the radar data matrix a person does not just occupy a fast-time index, but multiple fast-time indices. Generally speaking, indices occupied by the same person carry similar information of the person's vital signs. This phenomenon is called time diversity in wireless communication theory. Our MS-VMD algorithm employs time diversity, and jointly optimizes the problem of minimum bandwidth with multiple sequences taken into account, hence better than other algorithms (e.g. Hilbert-Huang transform [32], signal fitting [34] and traditional VMD algorithm [20]), where only one data sequence is considered.

We leverage this time diversity to reformulate the objective function of VMD according to [20]. Our modified VMD algorithm decomposes the data $z(t)$ into multiple Intrinsic Mode Functions(IMFs). We have $z(t) = \sum_{n=1}^{N} u_n(t)$ where $u_n(t)$ is the n-th IMF. However, for data of multiple lags (time delays in V²iFi) $z(t) = [z_1(t), z_2(t), \cdots, z_M(t)]^T$ where M represents the number of lags, we can obtain $\mathbf{z}(t) = \sum_{n=1}^{N} \mathbf{u}_n(t)$ where $\mathbf{u}_n(t) = [u_1(t) = u_n(t), u_2(t) = u_n(t), \cdots, u_M(t) = u_n(t)]^T$. Same as the conventional VMD, to estimate the bandwidth of IMFs, we need to follow the three steps: 1) each $\mathbf{u}_n(t)$ uses the Hilbert transform to compute the associated analytic signal, 2) $\mathbf{u}_n(t)$ is mixed with a complex exponential of center frequency ω_n to baseband, and 3) The bandwidth of $\mathbf{u}_n(t)$ can be estimated via the squared l^2-norm of the gradient. In this way, our constrained problem can be formulated as[2]:

$$\min_{u_n, \omega_n} \sum_{n=1}^{N} \sum_{m=1}^{M} \left\| \frac{\partial \left[\left(\delta(t) + \frac{j}{\pi t} \right) * u_n(t) \right] e^{-j\omega_n t}}{\partial t} \right\|_2^2$$

$$\text{s.t. } z_m(t) = \sum_{n=1}^{N} u_n(t), \ m = 1, 2, \cdots, M. \tag{4}$$

---

[2] j is the imaginary number unit, not the j as we used as frequency index in Section 3.4.1

Different from [20], the constraints become multiple linear equations corresponding to the number of lags. Therefore, the augmented Lagrangian function $\mathcal{L}$ is

$$
\mathcal{L} = \sum_{n=1}^{N} \sum_{m=1}^{M} \left\| \frac{\partial \left[\left(\delta(t) + \frac{j}{\pi t} \right) * u_n(t) \right] e^{-j\omega_n t}}{\partial t} \right\|_2^2 + \sum_{m=1}^{M} \left\| z_m(t) - \sum_{n=1}^{N} u_n(t) \right\|_2^2 + \sum_{m=1}^{M} \left\langle \lambda_m(t), z_m(t) - \sum_{n=1}^{N} u_n(t) \right\rangle.
\tag{5}
$$

Similar to [20], the E.q. (5) is also can be transformed to multiple simpler sub-optimization problems and solved by ADMM algorithm. Next, we divide the problem into two sub-problems: IMF update and center frequency update.

IMF update. We fix the center frequency ω_i firstly, and solve the minimization problem with respect to IMF $u_i(t)$. Then, we can obtain

$$
u_i^{q+1}(t) = \arg\min_{u_i} \left\| \frac{\partial \left[\left(\delta(t) + \frac{j}{\pi t} \right) * u_i(t) \right] e^{-j\omega_i t}}{\partial t} \right\|_2^2 + \sum_{m=1}^{M} \left\| z_m(t) - \sum_{n=1}^{N} u_n(t) + \frac{\lambda_m(t)}{2} \right\|_2^2,
\tag{6}
$$

where q is the current iteration.

According to Parseval/Plancherel Fourier isometry under the l^2-norm, the problem E.q. (6) is equal to solving the following problem in frequency domain:

$$
u_i^{q+1}(\omega) = \arg\min_{u_i} \| j\omega \left[(1 + \text{sgn}(\omega + \omega_i)) u_i(\omega + \omega_i) \right] \|_2^2 + \sum_{m=1}^{M} \left\| z_m(\omega) - \sum_{n=1}^{N} u_n(\omega) + \frac{\lambda_m(\omega)}{2} \right\|_2^2,
\tag{7}
$$

where $\text{sgn}(\cdot)$ is the sign function. We can use $\omega = \omega - \omega_i$ in the first term:

$$
u_i^{q+1}(\omega) = \arg\min_{u_i} \left\{ \int_{-\infty}^{+\infty} \left[4(\omega - \omega_i)^2 |u_i(\omega)|^2 + \sum_{m=1}^{M} \left| z_m(\omega) - \sum_{n=1}^{N} u_n(\omega) + \frac{\lambda_m(\omega)}{2} \right|^2 \right] d\omega \right\}.
\tag{8}
$$

We can rewrite both terms in E.q. (8) using half-space integrals over the non-negative frequencies, due to the Hermitian symmetry of real signals in the reconstruction term:

$$
u_i^{q+1}(\omega) = \arg\min_{u_i} \left\{ \int_0^{+\infty} \left[4(\omega - \omega_i)^2 |u_i(\omega)|^2 + 2 \sum_{m=1}^{M} \left| z_m(\omega) - \sum_{n=1}^{N} u_n(\omega) + \frac{\lambda_m(\omega)}{2} \right|^2 \right] d\omega \right\}.
\tag{9}
$$

Considering the problem E.q. (9) is to find the minimal function u_n, and then, according to the Euler-Lagrange equation [55] of the calculus of variations $\frac{\partial L}{\partial f} - \frac{d}{d\omega} \frac{\partial L}{\partial f'} = 0$, we can define

$$
L = 4(\omega - \omega_i)^2 |u_i(\omega)|^2 + 2 \sum_{m=1}^{M} \left| z_m(\omega) - \sum_{n=1}^{N} u_n(\omega) + \frac{\lambda_m(\omega)}{2} \right|^2 \text{ and } f = u_i(\omega).
\tag{10}
$$

Since f' is not explicit in L, the second term in the Euler-Lagrange equation vanishes. Thus, we let $\frac{\partial L}{\partial f} = 0$, and the first sub-problem can be solved

$$
\hat{u}_i^{q+1}(\omega) = \frac{\sum_{m=1}^{M} \left[\hat{z}_m(\omega) - \sum_{n \neq i} \hat{u}_n^{q+1}(\omega) + \frac{\hat{\lambda}_m(\omega)}{2} \right]}{M + 2(\omega - \omega_m)^2}.
\tag{11}
$$

Center frequency update. The center frequency ω_i is only related to the first term in E.q. (5), hence the second sub-problem is

$$\omega_i^{q+1} = \arg\min_{\omega_i} \left\| \frac{\partial \left[\left(\delta(t) + \frac{j}{\pi t} \right) * u_i(t) \right] e^{-j\omega_i t}}{\partial t} \right\|_2^2. \tag{12}$$

The optimization problem can also solved in frequency domain efficiently using the Plancherel theorem:

$$\omega_i^{q+1} = \arg\min_{\omega_i} \int_0^{+\infty} (\omega - \omega_i)^2 |\hat{u}_i(\omega)|^2 d\omega. \tag{13}$$

We also give the update expression at $(q+1)$-th iteration result as

$$\hat{\omega}_i^{q+1} = \frac{\int_0^\infty \omega |\hat{u}_i(\omega)|^2 d\omega}{\int_0^\infty |\hat{u}_i(\omega)|^2 d\omega}. \tag{14}$$

After that, we can plug the above two IMFs and center frequency updates into AMDD [8] to solve the MS-VMD problem. The complete MS-VMD algorithm is illustrated in Algorithm 1. Line 4 and line 6 are used to update $\hat{u}_i^{q+1}(\omega)$ and $\hat{\omega}_i^{q+1}$ according to E.q. (11) and E.q. (14), respectively in $(q+1)$-th iteration. In line 9, η is the update parameter. Line 11 is a condition to check convergence of this algorithm. Fig. 15 illustrates that our MS-VMD decompose the noisy signals into four modes, including respiration, heartbeat and other vehicle vibrations treated as noise components.

Algorithm 1: Complete MS-VMD

---

input : $\{\hat{u}_i^0\}$, $\{\hat{\omega}_i^0\}$, $\{\lambda_m^0\}$, $q \leftarrow 0$
output: $\{\hat{u}_i^q\}$, $\{\hat{\omega}_i^q\}$

1 **while** $q \leftarrow q + 1$ **do**
2   **for** $i \leftarrow 1$ **to** N **do**
3   *Update $\hat{u}_i$ for all $\omega \geq 0$:*
4          $\hat{u}_i^{q+1}(\omega) \leftarrow \dfrac{\sum_{m=1}^M \left[\hat{z}_m(\omega) - \sum_{n<i} \hat{u}_n^{q+1}(\omega) - \sum_{n>i} \hat{u}_n^q(\omega) \frac{\lambda_m^q(\omega)}{2} \right]}{M + 2(\omega - \omega_m)^2}$;
5   *Update $\hat{\omega}_i$:*
6          $\hat{\omega}_i^{q+1} \leftarrow \dfrac{\int_0^\infty \omega |\hat{u}_i(\omega)|^2 d\omega}{\int_0^\infty |\hat{u}_i(\omega)|^2 d\omega}$
7   **for** $m \leftarrow 1$ **to** M **do**
8   *Dual ascent for all $\omega \geq 0$:*
9          $\lambda_m^{q+1}(\omega) \leftarrow \lambda_m^q(\omega) + \eta \left(z_m(\omega) - \sum_n^N \hat{u}_n^{q+1}(\omega) \right)$;
10   *Convergence:*
11   **if** $\frac{\sum_n^N \|\hat{u}_n^{q+1} - \hat{u}_n^q\|_2^2}{\|\hat{u}\|_2^2} < \epsilon$ **then**
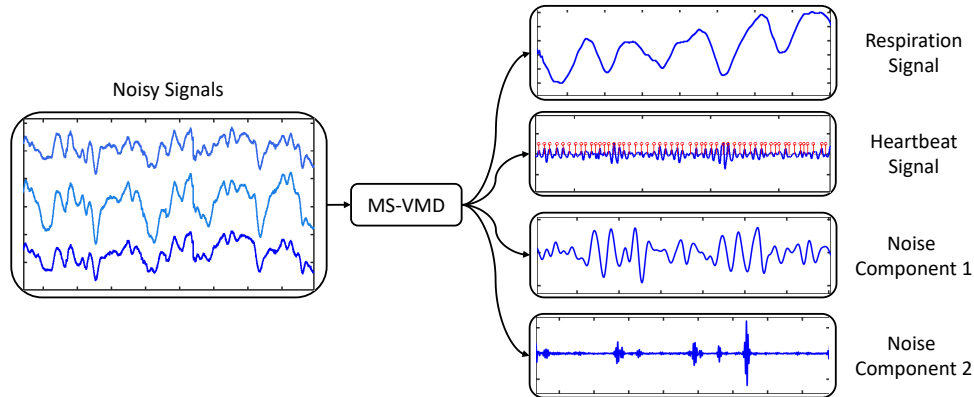12   break;

Fig. 15. Reflected signal decomposed by MS-VMD.

3.5 Vital Signs Extraction

So far we have decomposed the RF signal into its components, including respiration signal, heartbeat signal and noise caused by vehicle vibration. In this section, we introduce how we identify the respiratory and heartbeat component and extract vital signs.

3.5.1 Respiratory Rate Estimation. Respiration can be modeled as follows: when the driver or passengers inhales, his diaphragm and other related muscle contracts to create space in the lungs and the lungs expands and let the air flow in. Looking from outside, chest and abdomen of the driver move forward. If the impulse radio is placed at the front of the vehicle, chest and abdomen get closer to the impulse radio. Conversely, if the driver or passengers exhale, diaphragm and related muscles relax, therefore the space in the chest gets smaller and the air inside is squeezed out, his chest and abdomen move backward and further away from the device. Since the distance between human and V²iFi and the signal is linearly related, V²iFi can track the respiration of the driver or the passenger by detecting the amplitude. To determine the respiratory rate of the driver, we apply Fast Fourier Transform (FFT) to the IMFs obtained from MS-VMD. Since the frequency of respiration ranges from 0.16 Hz to 0.6 Hz, the component whose frequency matches the range is the respiratory component. And the peak frequency of this IMF is respiratory rate. Respiration is the blue line shown both in time domain and frequency domain in Fig. 16 and Fig. 17.

3.5.2 Heart Rate Estimation. Similar to respiration, the contraction and relaxation of human heart cause small displacements on the surface of different parts of the person's body. This phenomenon is called ventricular pump activity [45]. Ventricular pump activities are found in the head, torso, leg, buttock and etc. The minute movement caused by heartbeat also makes the signal change periodically, so V²iFi can also track heartbeat. To determine the heart rate of the driver, we again apply FFT to the IMFs obtained from MS-VMD (except the breathing-related IMF). Since the frequency of heartbeat ranges from 1 Hz to 2 Hz, the component whose frequency matches the range is the heartbeat component. And the peak frequency of this IMF is heart rate. Heartbeat is the red line shown both in time domain and frequency domain in Fig. 16 and Fig. 17.

3.5.3 Interbeat Interval Segmentation. To estimate interbeat intervals, we look into the heartbeat IMF, as shown in 16. IBIs are determined by the timings of each heartbeat. To obtain the exact timings, we detect peaks in the decomposed heartbeat IMF. However, the heartbeat waveform signal is weak and easily affected by noise and artifacts. Hence there are challenges in detecting peaks: i) heartbeat peak detection should be adaptive,
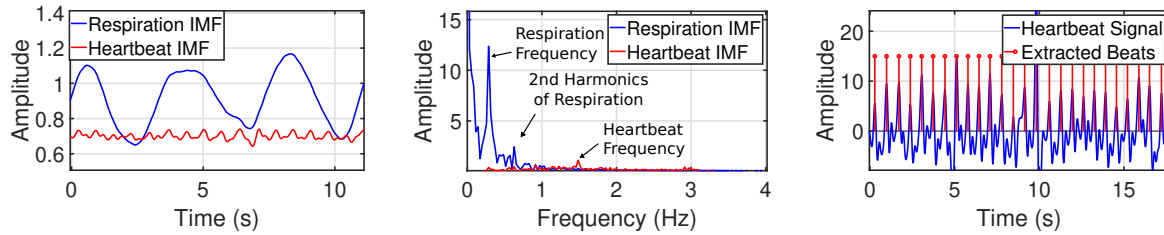
Fig. 16. Respiration and heartbeat IMFs in time domain.

Fig. 17. Respiration and heartbeat IMFs in frequency domain.

Fig. 18. Heartbeat signal and extracted timings of each beat.

since the strength of the signal is not stable and ii) fake peaks should be removed. To solve these challenges, we design a peak detection algorithm in which peaks are separated by at least $d_{\min}$ samples, that is to say, we find peaks that are the local maxima in a region of $2d_{\min} + 1$. $d_{\min}$ is determined by the heart rate estimated in Sec. 3.5.2. If the heart rate of the driver is HR, the heartbeat frequency is $HR/60$. Since the sampling rate of V^{2}iFi is 400 Hz, the average number of samples in one interval should be $N_{\mathrm{avg}} = HR \times 400/60$. The relation between the minimum samples in one IBI and the average samples is given by $N_{\min}^{\mathrm{IBI}} = cN_{\mathrm{avg}}^{\mathrm{IBI}}$, where c is a constant, and set to 0.7 empirically. To summarize, we detect local peaks separated by at least $0.7HR \times 400/60$ samples. The result of the peak detection algorithm is shown in Fig. 18. It can be seen that the timings of the beats are recovered accurately.

4 EVALUATION

In this section, we evaluate V^{2}iFi's performance by conducting road test. We tested on different road conditions, participants and procedures. As shown in Table 2, V^{2}iFi is able to measure respiratory rate, heart rate and heart rate variability for the driver, but it can only measure respiratory rate for all the other 3 people in the vehicle.

4.1 Experiment Setup

V^{2}iFi adopts a COTS impulse radio XETHRU [41] model X4M05 as its front-end. The radio transmits pulses with a width of 0.4 ns. The center frequency of the radio is 7.3 GHz, the bandwidth is 1.4 GHz, the sampling frequency is 23.328 GHz, and we set frame per second as 400. The radio is connected to a Raspberry Pi via Serial Peripheral Interface (SPI). The hardware PCB is rather small with a size of 6.5×3 cm^2. The whole hardware including power supply, 5 V fan, Raspberry Pi, and impulse radio is shown in Fig. 19. We place the whole V^{2}iFi on the windshield of a vehicle. Since the impulse radio is facing the driver (also shown in Fig. 19), it can capture maximum amount of weak signals from multiple body parts (e.g., chest, abdomen, forehead and neck). We implement the software system presented in Sec. 3 using C++; it operates in real-time.

Extensive road tests have been performed while developing V^{2}iFi. The driving route is designed to cover different road conditions and different traffic flows. Different conditions covered in the experiment include: parking, driving on smooth highway, driving on traffic-heavy road, driving in school area, driving at zebra and pedestrian crossing, entering and leaving intersections, driving uphill, driving downhill, driving in roundabouts, changing lanes, turning left, turning right and making U-turns. We have 4 drivers in total; each of them drive 15 miles and 30 minutes, so the total road test takes 60 miles and 2 hours. The vehicle used in the evaluation is a Mazda Axela. While the driver is driving, a copilot is responsible for collecting data. Two more passengers are in the back seats. We also tested effects of different clothing (lightweight T-shirt, heavyweight T-shirt, sweatshirt + lightweight T-shirt and sweatshirt + heavyweight T-shirt) on road tests.

Fig. 19. COTS impulse radio used in V²iFi and radio setup inside the vehicle.

We use a NEULOG respiration monitor belt logger sensor NUL-236 to obtain the ground truth of breathing. For heartbeat ground truth, we use the Heal Force PC-80B portable ECG monitor and extend the electrodes by exterior electrodes with lead wires to record the ECG data. The data is further processed to obtain heart rate and heart rate variability, which are then used as ground truth.

4.2 Overall Performance

4.2.1 Respiratory Rate Estimation Evaluation. Respiratory rate estimation error is used for the evaluation. The error is defined as the absolute value of the difference between the estimated respiratory rate R_E and the actual respiratory rate R_A, i.e., $|R_E - R_A|$. We evaluate the respiratory rate estimation performance of V²iFi against WiFind* and Leem et al. [34]. In WiFind*, we port the existing algorithm of WiFind [32] to UWB radio, so as to compare algorithms rather than radios. Leem et al. is one of the very few state-of-the-art research proposals leveraging UWB for vital sign detection [34]. Fig. 20(a) plots the CDF of respiratory rate measurement errors over all experiments. We can see that V²iFi achieves a median error of 0.06 rpm for the driver. As a comparison, the median error of respiratory rate of WiFind* and Leem et al. are 0.08 rpm and 0.06 rpm respectively, and they all have long tails indicating their performance is unstable in extreme conditions.

4.2.2 Heart Rate Estimation Evaluation. We evaluate the heart rate estimation performance of V²iFi against Leem et al. The heart rate estimation error is defined as the absolute value of the difference between the estimated heart rate R_E and the actual heart rate R_A, i.e., $|R_E - R_A|$. Fig. 20(b) plots the CDF of respiratory rate measurement errors over all experiments. We can see that V²iFi achieves a median error of 0.6 bpm for the driver. As a comparison, the median error of heart rate of Leem et al. [34] is 1.8 bpm, and has a relatively long tail indicating the performance is unstable in extreme conditions.

4.2.3 Heart Rate Variability Estimation Evaluation. Next, we evaluate V²iFi's heart rate variability estimation performance against Leem et al.. Since all other indicators, such as SDNN, SDRR, SDANN are all derived from IBI, we evaluate the accuracy of IBI measurement accuracy. Fig. 20(c) plots the CDF of IBI measurement errors over all experiments. We can see that V²iFi achieves a median error of 50 ms for the IBI of the driver. As a comparison, the median error of IBI of Leem et al. [34] is 166 ms, which is almost useless for vital sign monitoring.

4.2.4 Breathing and Heartbeat Transitions Evaluation. One thing to keep in mind is that V²iFi is designed for detecting abnormal human vital signs and alert the user when suspicious signals exist. Therefore it should not only detect normal signals, but also abnormal signals of the driver and passengers. Next we evaluate the performance of V²iFi for detecting abnormal vital signs. We ask the driver in the vehicle to intentionally change their respiratory rate (from 10 rpm to 15 rpm after 2 minutes) and respiration pattern. For heartbeat, we ask the
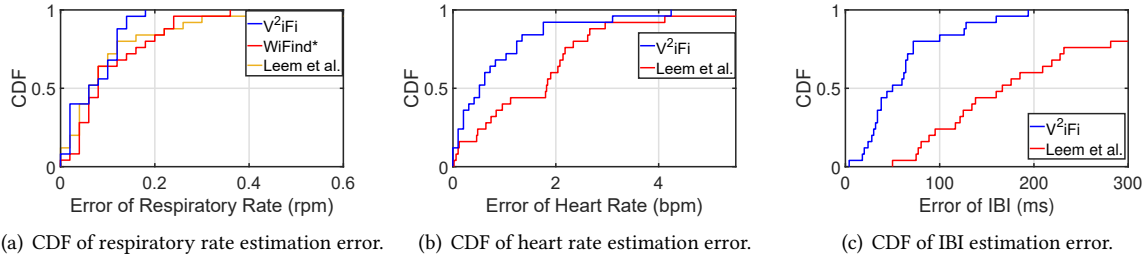
(a) CDF of respiratory rate estimation error.   (b) CDF of heart rate estimation error.   (c) CDF of IBI estimation error.

Fig. 20. Comparison of vital sign estimation performance among V^2iFi, WiFind* and Leem et al.

people in the vehicle to do some vigorous exercising to increase heart rate before entering the vehicle, and we observe how heart rate decreases with time. The result is shown in Fig. 21(a) and Fig. 21(b). It can be seen that the detected vital signs of V^2iFi follow the same trends as the actual abnormal vital signs for all these respiration heartbeat transitions. During the transitions, the average error of the estimated respiratory rate is 0.2 rpm, the average error of the estimated heart rate is 1.6 bpm.
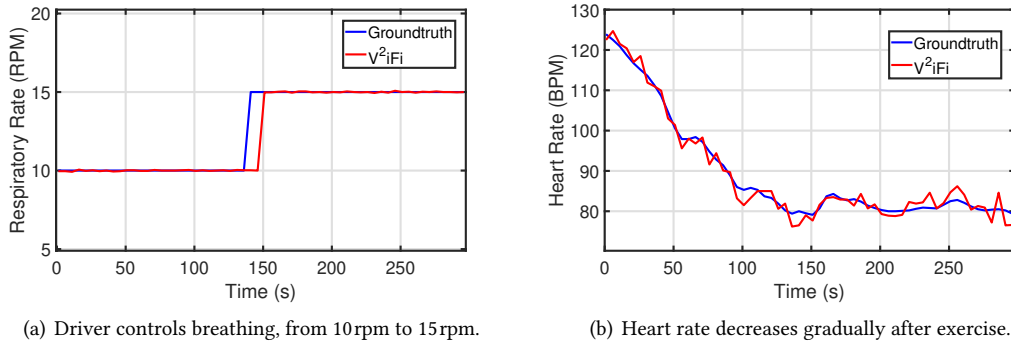

(a) Driver controls breathing, from 10 rpm to 15 rpm.   (b) Heart rate decreases gradually after exercise.

Fig. 21. Vital sign estimation performance of V^2iFi when respiratory rate and heart rate change.

4.3 User and Environment Issue Study

4.3.1 Number of Users. Although V^2iFi focuses on monitoring vital signs of the driver, the system can potentially be extended to monitor copilot and passengers in theory. In this section, we study the multi-user vital sign monitoring performance of V^2iFi. However, due to the Field of View (FOV) and noise in the vehicle, for the copilot and passengers, V^2iFi can measure respiratory rate only. Table 2 summarize the vital signs V^2iFi can measure for different users. In Fig. 22, it can be clearly seen that estimation error increases with distance, the respiratory rate estimation error of the driver is the smallest while passengers in the rear seats have the largest respiratory rate estimation error.

Table 2. Measured vital signs for different users.

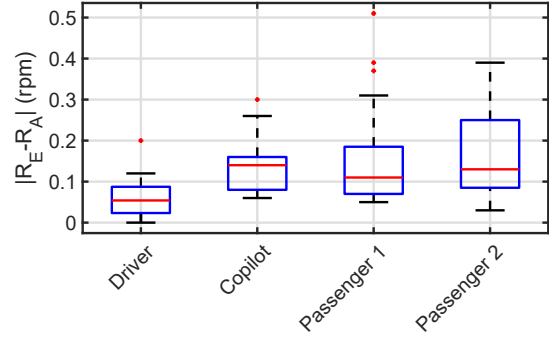|	Respiratory Rate	Heart Rate	Heart Rate Variability
Driver	Yes	Yes	Yes
Copilot	Yes	No	No
Passenger 1	Yes	No	No
Passenger 2	Yes	No	No

Fig. 22. Respiratory rate estimation error of different users.

4.3.2 Impact of Radio Placement. To get the best performance of V²iFi, we study the impact of different radio placements for V²iFi by placing the radio at three different locations in the vehicle, i.e., at the top of the windshield, at the bottom of the windshield, at the top of the chair and on the door. The estimation errors of the vital signs are shown in Fig. 23. It can be seen that the performance of V²iFi is the best when the radio is placed at the top of the windshield and faces the driver. In addition, when the radio is placed at the top of chair, the estimation errors of heart rate and IBI are relatively low. This is because when the impulse radio is placed at the top of the chair, it faces the driver's neck, where the carotid artery is located and movements caused by heartbeat is most obvious.

(a) Respiratory rate estimation error.

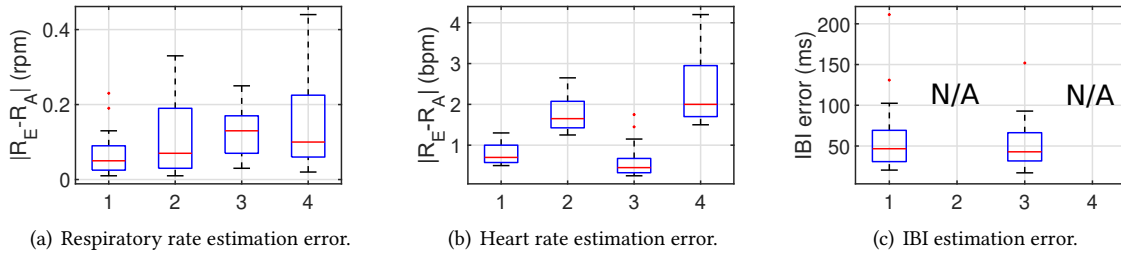(b) Heart rate estimation error.

(c) IBI estimation error.

Fig. 23. Respiratory rate, heart rate and IBI estimation error of the driver. In the figure, class 1 is the case the radio is mounted at the top of the windshield; class 2 is the case when the radio is mounted at the bottom of the windshield; class 3 is the case when the radar is mounted at the top of the chair; class 4 is the case when the radio is mounted on the door of the vehicle.

4.3.3 Impact of Clothing. In our experiment, we ask our driver to wear different clothes and observe their respective results. The performance of V²iFi is studied extensively under different clothing conditions. The clothing in our experiment are: (1) lightweight T-shirt (2) heavyweight T-shirt (3) sweatshirt +lightweight T-shirt (4) sweatshirt + heavyweight T-shirt. The result is shown in Fig. 24.

It can be seen for all the different clothing, V²iFi reaches a median estimation error 0.2 rpm for respiratory rate, a median estimation error 0.4 bpm for heart rate and 100 ms estimation error for IBI. Moreover, it can be seen that V²iFi performs better when the driver wear less, e.g., the result when the driver wear lightweight T-shirt is better than that of sweatshirt + heavyweight T-shirt. This is because some signals unable to penetrate heavyweight clothing and reach people's chest and abdomen and still able to detect minute movements like

heartbeat. Moreover, even in the worst case, where the driver or passenger wears sweatshirt + heavy weight T-shirt, the estimation error for respiratory rate and heart rate is still acceptable.

(a) Respiratory rate estimation error.   (b) Heart rate estimation error.   (c) IBI estimation error.
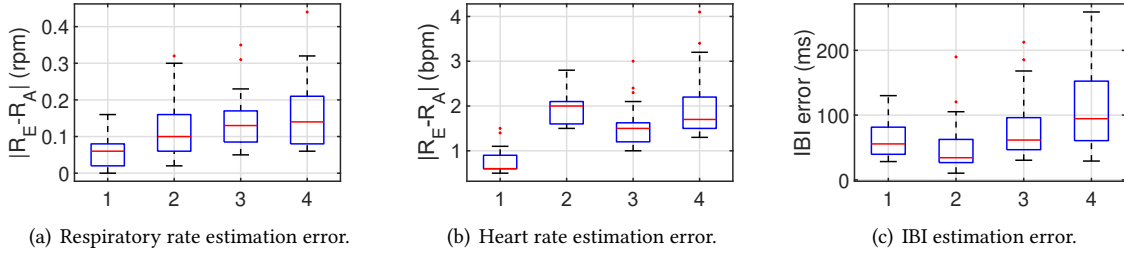
Fig. 24. Respiratory rate, heart rate and IBI estimation error of the driver. In the figure, class 1 is the case when the driver wear lightweight T-shirt; class 2 is the case when the driver wear heavyweight T-shirt; class 3 is the case when the driver wear sweatshirt + lightweight T-shirt; class 4 is the case when the driver wear sweatshirt + heavyweight T-shirt.

4.3.4 Impact of Road Types and Traffic Conditions. The signal quality of V^2iFi can be affect by different road types and traffic conditions, and thus the performance of V^2iFi can be impacted. To make sure V^2iFi works on different road types and under different traffic conditions. We collect data of different road types (e.g., smooth highway, bumpy road, uphill road, downhill road, intersections, left turns, right turns, roundabouts, U-turns) and analyzed the results respectively. The results are shown in Fig. 25. It can be seen that if the surface of the road is smooth and not many manoeuvres are made, the estimation error of vital signs are low, while bumpy roads and driving manoeuvres increase the estimation error.

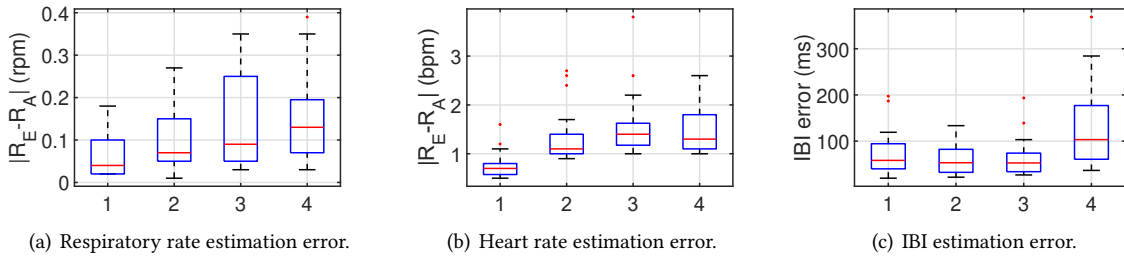(a) Respiratory rate estimation error.   (b) Heart rate estimation error.   (c) IBI estimation error.

Fig. 25. Respiratory rate, heart rate and IBI estimation error of the driver. In the figure, class 1 is the case when driving on smooth highway; class 2 is the case when driving uphill/downhill; class 3 is the case when taking turns (e.g., left turns, right turns, U-turns and roundabouts); class 4 is the case when driving on bumpy road.

4.4 Key Processes Study

4.4.1 Baseband Signal Processing. According to the analysis in Sec. 3, both amplitude and phase of the reflected signal after IQ downconversion contain vital sign information. V^2iFi chooses amplitude to estimate breathing and heartbeat. Contrary to common belief that amplitude is more vulnerable to random noises, our evaluation show that estimating vital signs by amplitude gives a better performance. Our explanation for this is as follows: if phase signal is to be used, we have to select a static fast-time bin as reference and do phase correction first.

However, in driving environments, it is nearly impossible to find fast-time bin which represents a static reflector. Therefore, in V^{2}iFi, amplitude of the baseband signal is selected for vital sign extraction.

(a) Respiratory rate estimation error.   (b) Heart rate estimation error.   (c) IBI estimation error.
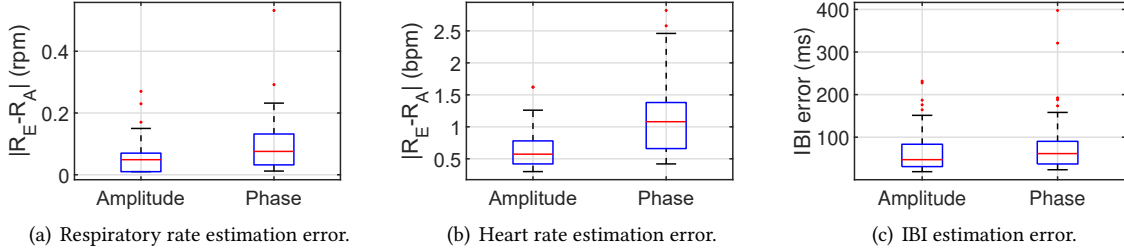
Fig. 26. Respiratory rate, heart rate and IBI estimation error of using the amplitude and phase of the baseband signal.

The experiment result is shown in Fig. 26. It can be seen that system using amplitude signal achieves less overall errors than systems using phase signal. For respiratory rate estimation error, the median with amplitude baseband processing is 0.06 rpm, and the median with phase baseband processing is 0.08 rpm. For heart rate estimation error, the median with amplitude baseband processing is 0.6 bpm, and the median with phase baseband processing is 1.1 bpm. For IBI estimation error, the median with amplitude baseband processing is 50 ms, and median with phase baseband processing is 60 ms.

4.4.2 Signal Decomposition. In V^{2}iFi, our novel MS-VMD algorithm is used to decompose the filtered signal into its vital sign components. According to the analysis in Sec. 3.4, our novel MS-VMD algorithm employs time diversity to enhance vital signals. It jointly optimizes the problem of minimum bandwidth with multiple sequences taken into account, hence better than VMD, where only one data sequence is considered. Fig. 27 gives the resulting waveforms of a case where conventional VMD algorithm only obtains a mix of respiration and heartbeat, while MS-VMD separates the two signals successfully.

(a) Decomposition result of VMD.   (b) Decomposition result of MS-VMD.

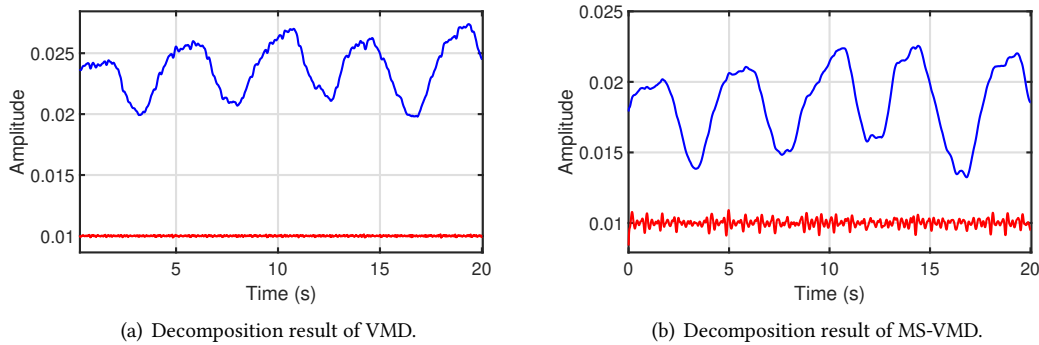Fig. 27. Example of VMD and MS-VMD on decomposing signals to respiration and heartbeat component.

To evaluate their performance, we test these two algorithms on the same data, and the result is shown in Fig. 28. In the figure, it can be seen that system using MS-VMD algorithm achieves less overall errors than systems using VMD algorithm. For respiratory rate estimation error, the median with MS-VMD algorithm is 0.06 rpm, and the

median with VMD algorithm is 0.07 rpm. For heart rate estimation error, the median with MS-VMD algorithm is 0.6 bpm, and the median with VMD algorithm is 0.8 bpm. For IBI estimation error, the median with MS-VMD algorithm is 50 ms, and the median with VMD algorithm is 100 ms.

(a) Respiratory rate estimation error.   (b) Heart rate estimation error.   (c) IBI estimation error.
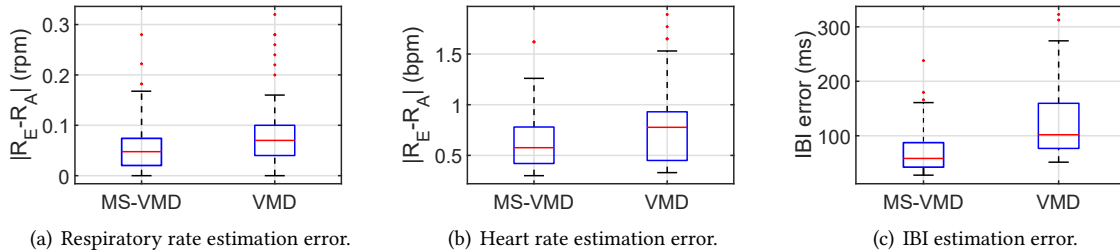
Fig. 28. Respiratory rate, heart rate and IBI estimation error of MS-VMD algorithm and VMD algorithm.

5   LIMITATIONS AND POTENTIALS

5.1   Limitation of V^{2}iFi

We designed V^{2}iFi in the hope of bringing well-being to the driving environments. V^{2}iFi is successful in terms of monitoring vital signs. However, monitoring is not the final goal: the vital sign data collected should be used by the vehicle to infer user states and take actions correspondingly. To achieve this, vital signs should be mapped to physiological and psychological states. In previous studies it is shown that the vital signs can indeed reflect physical health (e.g., cadiac health and drowsiness level) [16, 25, 35] and mental health (e.g., emotion and mental workload) [9, 65]. A commonly used approach for such mapping is supervised learning, e.g., decision tree and SVM [32]. However, learning algorithms do not work without properly labelled data. Awais et al. [3] use subjective measures (i.e., what the participant says) to label both physical and mental states, but subjective measures are unreliable and inaccurate, potentially leading to inconsistent inference results. To measure the person-specific states objectively and accurately, we face many challenges such as infringement of privacy and lack of gauging device. Moreover, medical organizations do not easily provide related data because of potential misuse of information and violation of law. Nevertheless, once we have properly labelled data at hand, we envision that V^{2}iFi can become the foundation of more interesting applications, as we present in the following.

5.2   Application 1: Driver Drowsiness Detection

Driver drowsiness is one of the biggest culprit in car accidents, research shows that driver drowsiness is a contributing factor in 20% of all the crashes [31], and about 25% of all fatalities on road [26]. A series of vital sign changes indicate a drowsy driver, e.g., decreased respiratory rate, decreased heart rate and decreased HRV. V^{2}iFi can detect all these changes, and a high-level learning algorithm such as decision tree and SVM can be used to combine the aforementioned change in vital signs to make a binary decision(i.e., drowsy or awake) in a specific time span. An example decision tree is shown in Fig. 29.

5.3   Application 2: Road Rage Prevention

Road rage is violent behaviors perpetrated by drivers and it is extremely dangerous. Being slowed down and blocked by others on overly crowded streets make drivers on the road irritated and road rage arises thereafter. DePasquale et al. [19] show road rage incidents is on the rise in recent years. To prevent road rage, legal measures,
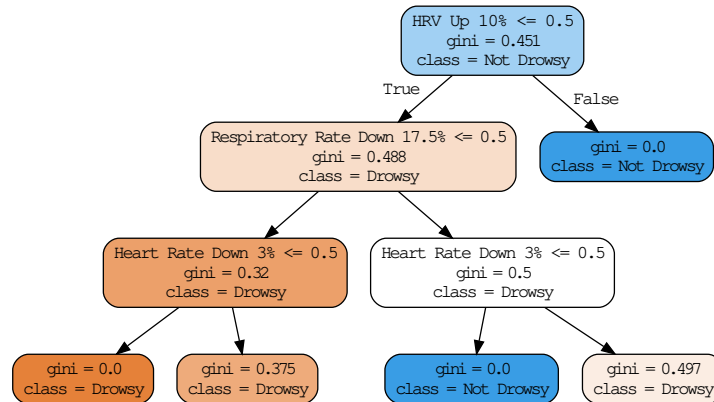
Fig. 29. Driver drowsiness decision tree: an example.

better vehicle design, education in everyday life and infrastructure improvement have been tested. However, because road rage events are sporadic, all these preventive measures cannot handle a real road rage event in time. Since reflected RF signals of V²iFi carry information of the emotion of the driver [65], it is possible to build a road rage detection system on top of V²iFi and the vehicle can respond, take precautions and combat road rage. Similar to driver drowsiness detection, we can use a learning algorithm, such as a decision tree similar to that in Fig. 29 to infer the driver's road rage level. The vehicle can then sends an alert to the driver in time or brakes if necessary.

5.4 Application 3: Health Monitoring for Children and Seniors in the Vehicle

It has long been known that environments inside vehicle cause significant health harm and hazards. Particularly, seniors and children are more vulnerable and tend to become victims. There are two reasons: i) seniors and children are more physically inactive inside a vehicle and ii) children and seniors are more sensitive to the car exhaust in vehicle. With V²iFi, vital signs of children and seniors inside can be monitored, and common diseases such as childhood asthma and heart failure among the senior people can be infered from abnormal vital signs, hence be prevented. V²iFi is a potential solution to solve the health issues and build a healthy and secure environments for the children and seniors.

6 RELATED WORK

Existing work in health monitoring in driving environments can be roughly categorized into three classes: (1) vision-based method, (2) sensor-based method and (3) RF-based method.

The accuracy of the detection systems depends largely on the invasiveness allowed. The detection systems with direct contact with the driver are the most accurate ones, but they hinder the body movements of the driver and thus cause inconvenience while driving, so they are not accepted very well in the industry. On the other side of the invasiveness spectrum are those "aerial" sensors, they are not in direct contact with the driver. These systems get indirect signals of the driver, such as eye movement to infer other physiological variables, so they cannot be very accurate. Although these systems are more easily accepted in the industry, they need more data and calibration to characterize health states of the people effectively. In the following, we elaborate the subcategories of the systems:

Vision-based methods: Vision-based methods deploy one camera, usually at the front of the vehicle, to capture the activities, various signals and performance of the driver and passengers. Eriksson et al. [23] proposed a system to track movements of eyes and eyelids of the driver. Following preprocessing, they locate the driver's face in the grayscale image, and then eyes are further located and tracked. The states of the eyes, whether open or closed are determined by template matching. However, taking photo of the driver's face raises privacy concerns, which makes it not good for private room such as driving environments. Meanwhile, vision-based systems are also sensible to external conditions, lighting and weather conditions, different dress and fashion accessories like glasses, winter clothes will decrease the detection accuracy.

Sensor-based methods: Sensor-based methods can be further categorized to two groups: EEG-based and ECG-based method. EEG-based methods use brain physiological changes to detect vital signs. Multiple thin metal wires (electrodes) are placed on the scalp. The waveform obtained by EEG reflects the mental activities of the brain. In [39], nonlinear and chaotic vital signs of drivers are extracted. Another portable low-cost EEG method is proposed in [43], and SVM is used to classify EEG data as different health states. Similar to EEG-based methods, ECG-based methods provide accurate physiological signals of the driver under test. Heart rate variability is extracted from the ECG signal in [22, 56]. In another work, a smart cushion containing an integrated micro-bending fiber sensor is used to imitate ECG sensors [18]. However, EEG and ECG deploy sensors on human skin to detect biological signals. They require conductive paste to reduce skin impedance to build electrical contact, making the methods intrusive, time-consuming and inconsistent when long recording is needed [54]. These methods always make the users aware of its existence and degrade user experience.

Wi-Fi-based methods: Wi-Fi sensing based vital sign estimation has been investigated in recent works such as [58, 61, 63, 64]. These works focus on static environment but not in-vehicle environment. In [32], Jia et al. propose a fatigue detection approach Wi-Find based on Wi-Fi CSI. Channel State Information (CSI) describes the channel properties of a communication link from the transmitter to the receiver. For a Wi-Fi router, CSI information can be obtained at different carrier frequencies and along different paths. The CSI measured by Wi-Fi devices is widely used for localization, occupation sensing, activity recognition and other sensing purposes. Compared to the aforementioned sensor-based systems, the system proposed in [32] only requires a wireless STA and AP, thus is device-free.

Despite the existence of several vital signs monitoring systems, few of them are practical in the driving environments. Our work answers challenges such as passenger interference, in-vehicle vibration, human motion, etc., and monitors vital signs in driving environments successfully.

7 CONCLUSION

In this paper, we present the design and implementation of V^2iFi, which a vital sign monitoring system in driving environments leveraging the power of impulse radio. We address several challenges including extracting fine-grained driver's vital sign from RF signal polluted with vehicle vibration noise and mixed with vital signals from other passengers. V^2iFi consists of multiple algorithms for removing noise, including the novel MS-VMD algorithm. The system is evaluated in real road test and demonstrated low respiratory rate, heart rate and heart rate variability estimation error. In the future, we will extend V^2iFi to a fully-grown in-vehicle health monitoring system. We believe V^2iFi takes a big step toward enabling health monitoring in driving environments, it allows vehicles to "listen" and understand the driver and passengers and thus become more intelligent.

ACKNOWLEDGMENTS

REFERENCES

[1] Fadel Adib, Zach Kabelac, Dina Katabi, and Robert C Miller. 2014. 3D Tracking via Body Radio Reflections. In *Proc. of the 10th USENIX NSDI*. 317–329.

[2] Fadel Adib, Hongzi Mao, Zachary Kabelac, Dina Katabi, and Robert C Miller. 2015. Smart Homes That Monitor Breathing and Heart Rate. In *Proc. of the 33rd ACM CHI*. 837–846.

[3] Muhammad Awais, Nasreen Badruddin, and Micheal Drieberg. 2017. A Hybrid Approach to Detect Driver Drowsiness Utilizing Physiological Signals to Improve System Performance and Wearability. *Sensors* 17, 9 (2017), 1991.

[4] Amerjeet S Banning and G Andre Ng. 2012. Driving and Arrhythmia: A Review of Scientific Basis for International Guidelines. *European Heart Journal* 34, 3 (2012), 236–244.

[5] Thomas Benichou, Bruno Pereira, Martial Mermillod, Igor Tauveron, Daniela Pfabigan, Salwan Maqdasy, and Frederic Dutheil. 2018. Heart Rate Variability in Type 2 Diabetes Mellitus: A Systematic Review and Meta-Analysis. *PLOS One* 13, 4 (2018), e0195166.

[6] Svante Björklund, Anders Nelander, and Mats I Pettersson. 2015. Fast-Time and Slow-Time Space-Time Adaptive Processing for Bistatic Radar Interference Suppression. In *2015 IEEE Radar Conference (Radarcon)*. 0674–0678.

[7] BMW AG. 2019. Smartsenior: Intelligente Dienste Und Dienstleistungen Für Senioren. http://www1.smart-senior.de/pdf/presse/SmartSenior_CeBIT_Partnerflyer_BMW_DE_EN_2012_final.pdf. Accessed: 2019-10-09.

[8] Stephen Boyd, Neal Parikh, Eric Chu, Borja Peleato, Jonathan Eckstein, et al. 2011. Distributed Optimization and Statistical Learning via the Alternating Direction Method of Multipliers. *Foundations and Trends® in Machine learning* 3, 1 (2011), 1–122.

[9] Karel A Brookhuis and Dick de Waard. 2010. Monitoring Drivers' Mental Workload in Driving Simulators using Physiological Measures. *Accident Analysis & Prevention* 42, 3 (2010), 898–903.

[10] JR Catterall, PMA Calverley, V Brezinova, NJ Douglas, HM Brash, CM Shapiro, and DC Flenley. 1982. Irregular Breathing and Hypoxaemia During Sleep in Chronic Stable Asthma. *The Lancet* 319, 8267 (1982), 301–304.

[11] John A Chalmers, Daniel S Quintana, Maree J Abbott, Andrew H Kemp, et al. 2014. Anxiety Disorders Are Associated with Reduced Heart Rate Variability: A Meta-Analysis. *Frontiers in Psychiatry* 5 (2014), 80.

[12] Hyunggi Cho, Young-Woo Seo, BVK Vijaya Kumar, and Ragunathan Raj Rajkumar. 2014. A Multi-Sensor Fusion System for Moving Object Detection and Tracking in Urban Driving Environments. In *IEEE International Conference on Robotics and Automation (ICRA)*. 1836–1843.

[13] Eric Chern-Pin Chua, Wen-Qi Tan, Sing-Chen Yeo, Pauline Lau, Ivan Lee, Ivan Ho Mien, Kathiravelu Puvanendran, and Joshua J. Gooley. 2012. Heart Rate Variability Can Be Used to Estimate Sleepiness-related Decrements in Psychomotor Vigilance during Total Sleep Deprivation. *Sleep* 35, 3 (03 2012), 325–334.

[14] Vivian L Clark and James A Kruse. 1990. Clinical Methods: The History, Physical, and Laboratory Examinations. *Jama* 264, 21 (1990), 2808–2809.

[15] Michelle A Cretikos, Rinaldo Bellomo, Ken Hillman, Jack Chen, Simon Finfer, and Arthas Flabouris. 2008. Respiratory Rate: The Neglected Vital Sign. *Medical Journal of Australia* 188, 11 (2008), 657–659.

[16] Dirk Cysarz, Silke Lange, Peter F Matthiessen, and Peter van Leeuwen. 2007. Regular Heartbeat Dynamics Are Associated with Cardiac Health. *Am. J. Physiol* 292, 1 (2007), R368–R372.

[17] Daimler AG. 2019. Attention Assist: Drowsiness-Detection System Warns Drivers to Prevent Them Falling Asleep Momentarily - Daimler Global Media Site. https://media.daimler.com/marsMediaSite/en/instance/ko/ATTENTION-ASSIST-Drowsiness-detection-system-warns-drivers-to-prevent-them-falling-asleep-momentarily.xhtml?oid=9361586. Accessed: 2019-10-09.

[18] Chacko John Deepu, Zhihao Chen, Ju Teng Teo, Soon Huat Ng, Xiefeng Yang, and Yong Lian. 2012. A Smart Cushion for Real-Time Heart Rate Monitoring. In *2012 IEEE Biomedical Circuits and Systems Conference*. 53–56.

[19] Jason P DePasquale, E Scott Geller, Steven W Clarke, and Lawrence C Littleton. 2001. Measuring Road Rage: Development of The Propensity for Angry Driving Scale. *J. Saf. Res.* 32, 1 (2001), 1–16.

[20] Konstantin Dragomiretskiy and Dominique Zosso. 2013. Variational Mode Decomposition. *IEEE Transactions on Signal Processing* 62, 3 (2013), 531–544.

[21] Malcolm Elliott and Alysia Coventry. 2012. Critical Care: the Eight Vital Signs of Patient Monitoring. *British Journal of Nursing* 21, 10 (2012), 621–625.

[22] Sigrid Elsenbruch, Michael J Harnish, and William C Orr. 1999. Heart Rate Variability During Waking and Sleep in Healthy Males and Females. *Sleep* 22, 8 (1999), 1067–1071.

[23] Martin Eriksson and Nikolaos P Papanikotopoulos. 1997. Eye-Tracking for Detection of Driver Fatigue. In *Proc. of Conference on Intelligent Transportation Systems*. 314–319.

[24] Gernot Ernst. 2017. Heart-Rate Variability-More than Heart Beats? *Frontiers in Public Health* 5 (2017), 240.

[25] John F Fieselmann, Michael S Hendryx, Charles M Helms, and Douglas S Wakefield. 1993. Respiratory Rate Predicts Cardiopulmonary Arrest for Internal Medicine Inpatients. *Journal of General Internal Medicine* 8, 7 (1993), 354–360.

[26] Diane Flatley, LA Reyner, and James A Horne. 2004. Sleep-Related Crashes on Sections of Different Road Types in the UK (1995-2001). *Road Safety United States Naval School of Aviation Medicine 52* (2004).

[27] Koichi Fujiwara, Erika Abe, Keisuke Kamata, Chikao Nakayama, Yoko Suzuki, Toshitaka Yamakawa, Toshihiro Hiraoka, Manabu Kano, Yukiyoshi Sumi, Fumi Masuda, et al. 2018. Heart Rate Variability-Based Driver Drowsiness Detection and its Validation with EEG. *IEEE Transactions on Biomedical Engineering* 66, 6 (2018), 1769–1778.

[28] Nicholas D Giardino, Seth D Friedman, and Stephen R Dager. 2007. Anxiety, Respiration, and Cerebral Blood Flow: Implications for Functional Brain Imaging. *Comprehensive Psychiatry* 48, 2 (2007), 103–112.

[29] Daniel Halperin, Wenjun Hu, Anmol Sheth, and David Wetherall. 2011. Tool Release: Gathering 802.11n Traces with Channel State Information. *ACM SIGCOMM Computer Communication Review* 41, 1 (2011), 53.

[30] Sinh Huynh, Rajesh Krishna Balan, JeongGil Ko, and Youngki Lee. 2019. VitaMon: Measuring Heart Rate Variability Using Smartphone Front Camera. In *Proc. of the 17th ACM Sensys.* 1–14.

[31] P Jackson, C Hilditch, A Holmes, N Reed, N Merat, and L Smith. 2011. Fatigue and Road Safety: A Critical Analysis of Recent Evidence. *Department for Transport, Road Safety Web Publication* 21 (2011).

[32] Wenjia Jia, Hongjian Peng, Na Ruan, Zhiping Tang, and Wei Zhao. 2018. WiFind: Driver Fatigue Detection with Fine-Grained Wi-Fi Signal Features. *IEEE Transactions on Big Data* (2018), 1–14.

[33] Sang-Ho Jo, Jin-Myung Kim, and Dong Kyoo Kim. 2019. Heart Rate Change While Drowsy Driving. *Journal of Korean Medical Science* 34, 8 (2019).

[34] Seong Kyu Leem, Faheem Khan, and Sung Ho Cho. 2017. Vital Sign Monitoring and Mobile Phone Usage Detection Using IR-UWB Radar for Intended Use in Car Crash Prevention. *Sensors* (2017).

[35] Gang Li, Boon-Leng Lee, and Wan-Young Chung. 2015. Smartwatch-based Wearable EEG System for Driver Drowsiness Detection. *IEEE Sensors Journal* 15, 12 (2015), 7169–7180.

[36] Xiang Li, Daqing Zhang, Qin Lv, Jie Xiong, Shengjie Li, Yue Zhang, and Hong Mei. 2017. IndoTrack: Device-Free Indoor Human Tracking with Commodity Wi-Fi. *Proc. of the 17th ACM UbiComp* 1, 3 (2017), 72.

[37] H-O Lisper, Hans Laurell, and G Stening. 1973. Effects of Experience of The Driver on Heart-Rate, Respiration-Rate, and Subsidiary Reaction Time in A Three Hours Continuous Driving Task. *Ergonomics* 16, 4 (1973), 501–506.

[38] Mohamed Faisal Lutfi. 2015. Patterns of Heart Rate Variability and Cardiac Autonomic Modulations in Controlled and Uncontrolled Asthmatic Patients. *BMC Pulmonary Medicine* 15, 1 (2015), 119.

[39] Zahra Mardi, Seyedeh Naghmeh Miri Ashtiani, and Mohammad Mikaili. 2011. EEG-Based Drowsiness Detection for Safe Driving Using Chaotic Features and Statistical Tests. *Journal of Medical Signals and Sensors* 1, 2 (2011), 130.

[40] Hermann Nabi, Martica Hall, Markku Koskenvuo, Archana Singh-Manoux, Tuula Oksanen, Sakari Suominen, Mika Kivimäki, and Jussi Vahtera. 2010. Psychological and Somatic Symptoms of Anxiety and Risk of Coronary Heart Disease: the Health and Social Support Prospective Cohort Study. *Biological Psychiatry* 67, 4 (2010), 378–385.

[41] Novelda AS. 2017. Single-Chip Radar Sensors with Sub-mm Resolution - XETHRU. https://www.xethru.com/. Accessed: 2019-10-03.

[42] Novelda AS. 2017. XETHRU Sensor Emissions: An In-Depth Look at Radar Safety Regulations. https://www.xethru.com/blog/posts/xethru-radar-emission-comparison. Accessed: 2019-10-03.

[43] Mikito Ogino and Yasue Mitsukura. 2018. Portable Drowsiness Detection Through Use of A Prefrontal Single-Channel Electroencephalogram. *Sensors* 18, 12 (2018), 4477.

[44] Jin-Kwan Park, Yunseog Hong, Hyunjae Lee, Chorom Jang, Gi-Ho Yun, Hee-Jo Lee, and Jong-Gwan Yook. 2019. Noncontact RF Vital Sign Sensor for Continuous Monitoring of Driver Status. *IEEE Transactions on Biomedical Circuits and Systems* 13, 3 (2019), 493–502.

[45] Eduardo Pinheiro, Octavian Postolache, and Pedro Girão. 2010. Theory and Developments in An Unobtrusive Cardiovascular System Representation: Ballistocardiography. *The Open Biomedical Engineering Journal* 4 (2010), 201.

[46] Harold R Raemer. 1996. *Radar Systems Principles.* CRC press.

[47] Raspberry Pi Foundation. 2019. Teach, Learn and Make with Raspberry Pi - Raspberry Pi. https://https://www.raspberrypi.org/. Accessed: 2019-10-03.

[48] Francesco Sessa, Valenzano Anna, Giovanni Messina, Giuseppe Cibelli, Vincenzo Monda, Gabriella Marsala, Maria Ruberto, Antonio Biondi, Orazio Cascio, Giuseppe Bertozzi, et al. 2018. Heart Rate Variability As Predictive Factor for Sudden Cardiac Death. *Aging (Albany NY)* 10, 2 (2018), 166.

[49] Fred Shaffer and JP Ginsberg. 2017. An Overview of Heart Rate Variability Metrics and Norms. *Frontiers in Public Health* 5 (2017), 258.

[50] Fred Shaffer, Rollin McCraty, and Christopher L Zerr. 2014. A Healthy Heart Is Not A Metronome: An Integrative Review of the Heart's Anatomy and Heart Rate Variability. *Frontiers in Psychology* 5 (2014), 1040.

[51] Anupriya Sharma, NB Hirulkar, and Payal Ranka. 2011. Effect of Hyperglycemia on Electrolytes Imbalance. *Int J Pharm Biol Arch* 2 (2011), 526–33.

[52] José Solaz, José Laparra-Hernández, Daniel Bande, Noelia Rodríguez, Sergio Veleff, José Gerpe, and Enrique Medina. 2016. Drowsiness Detection Based on the Analysis of Breathing Rate Obtained from Real-Time Image Recognition. *Transportation Research Procedia* 14 (2016), 3867–3876.

[53] Richard Strauß, Santiago Ewig, Klaus Richter, Thomas König, Günther Heller, and Torsten T Bauer. 2014. The Prognostic Significance of Respiratory Rate in Patients with Pneumonia: A Retrospective Analysis of Data from 705 928 Hospitalized Patients in Germany from 2010–2012. *Deutsches Ärzteblatt International* 111, 29-30 (2014), 503.

[54] Thomas J Sullivan, Stephen R Deiss, and Gert Cauwenberghs. 2007. A Low-Noise, Non-Contact EEG/ECG Sensor. In *2007 IEEE Biomedical Circuits and Systems Conference*. 154–157.

[55] John L Troutman. 2012. *Variational Calculus and Optimal Control: Optimization with Elementary Convexity.* Springer Science & Business Media.

[56] Mihoko Tsunoda, Takuro Endo, Satoko Hashimoto, Sato Honma, and Ken-Ichi Honma. 2001. Effects of Light and Sleep Stages on Heart Rate Variability in Humans. *Psychiatry and Clinical Neurosciences* 55, 3 (2001), 285–286.

[57] Volvo Group. 2019. Driver Alert System. https://www.volvocars.com/en-th/support/manuals/s60/2014/driver-support/driver-alert-system/driver-alert-control-dac---operation. Accessed: 2019-10-09.

[58] Chuyu Wang, Lei Xie, Wei Wang, Yingying Chen, Yanling Bu, and Sanglu Lu. 2018. RF-ECG: Heart Rate Variability Assessment Based on COTS RFID Tag Array. *Proc. of the 17th ACM UbiComp* 2, 2 (2018), 85.

[59] Tianben Wang, Daqing Zhang, Yuanqing Zheng, Tao Gu, Xingshe Zhou, and Bernadette Dorizzi. 2018. C-FMCW Based Contactless Respiration Detection Using Acoustic Signal. *Proc. of the 17th ACM UbiComp* 1, 4 (2018), 170.

[60] WS Waring, JY Rhee, DN Bateman, GE Leggett, and H Jamie. 2008. Impaired Heart Rate Variability and Altered Cardiac Sympathovagal Balance After Antidepressant Overdose. *European Journal of Clinical Pharmacology* 64, 11 (2008), 1037–1041.

[61] Dan Wu, Daqing Zhang, Chenren Xu, Hao Wang, and Xiang Li. 2017. Device-Free WiFi Human Sensing: From Pattern-Based to Model-Based Approaches. *IEEE Communications Magazine* 55, 10 (2017), 91–97.

[62] Xiangyu Xu, Jiadi Yu, Yingying Chen, Yanmin Zhu, Linghe Kong, and Minglu Li. 2019. BreathListener: Fine-Grained Breathing Monitoring in Driving Environments Utilizing Acoustic Signals. In *Proc. of the 17th ACM MobiSys*. 54–66.

[63] Youwei Zeng, Dan Wu, Ruiyang Gao, Tao Gu, and Daqing Zhang. 2018. FullBreathe: Full Human Respiration Detection Exploiting Complementarity of CSI Phase and Amplitude of WiFi Signals. *Proc. of the 18th ACM UbiComp* 2, 3 (2018), 148.

[64] Jin Zhang, Weitao Xu, Wen Hu, and Salil S Kanhere. 2017. WiCare: Towards In-Situ Breath Monitoring. In *Proc. of the 14th ACM MobiQuitous*. ACM, 126–135.

[65] Mingmin Zhao, Fadel Adib, and Dina Katabi. 2016. Emotion Recognition Using Wireless Signals. In *Proc. of the 22nd ACM MobiCom*. 95–108.